Medical Imaging with AI

Hyunna Lee

Medical Imaging & Intelligent Reality Lab (MI2RL)
Health Innovation Big Data Center, Asan Medical Center
South Korea

인공지능 기술의 혁신: 딥러닝

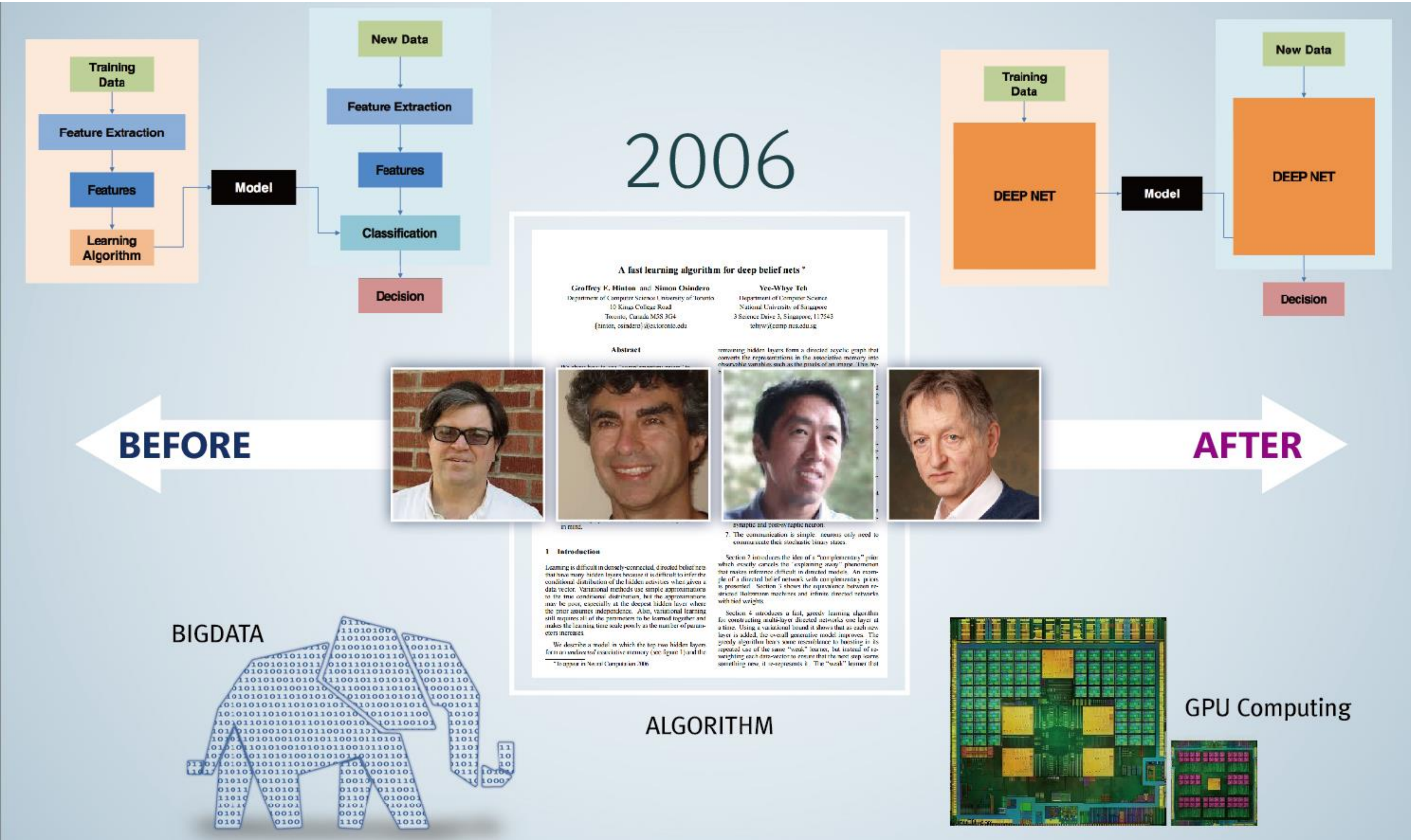

인공지능 기술의 혁신: 딥러닝

Speech Recognition

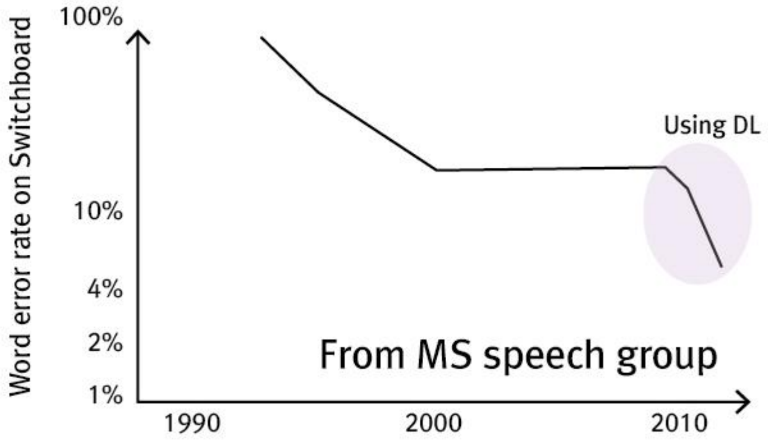

Object (Image) Recognition (ImageNet)

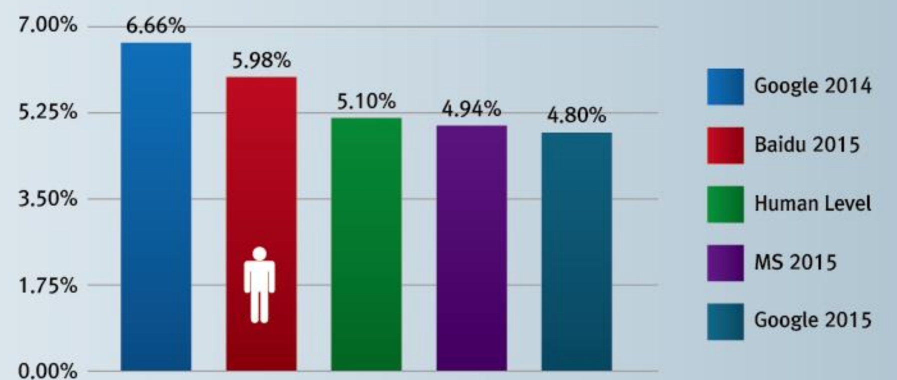

Face Verification

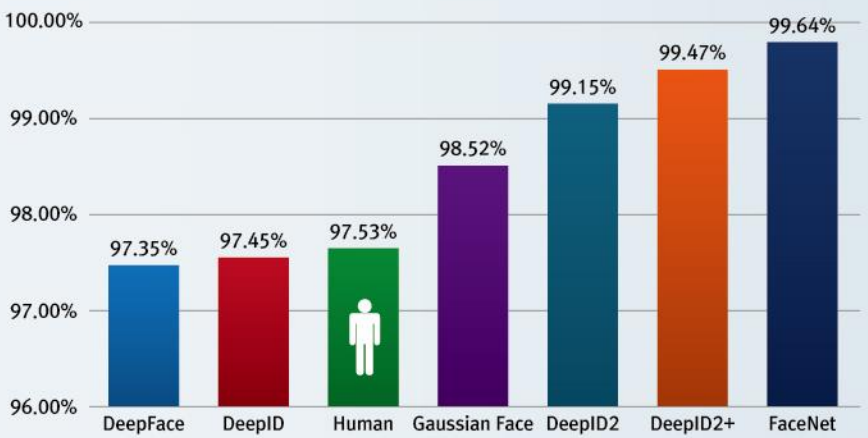

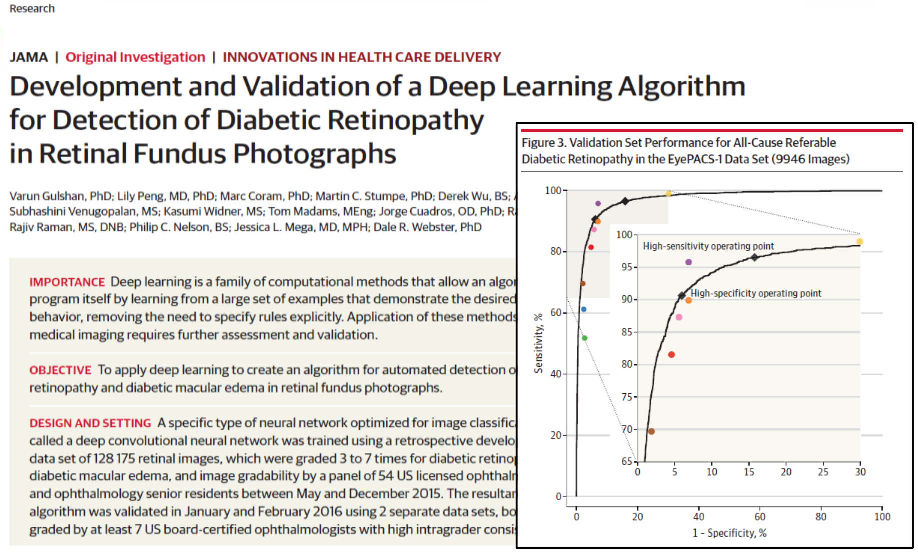
Research

JAMA | Original Investigation | INNOVATIONS IN HEALTH CARE DELIVERY

Development and Validation of a Deep Learning Algorithm for Detection of Diabetic Retinopathy in Retinal Fundus Photographs

Varun Gulshan, PhD; Lily Peng, MD, PhD; Marc Coram, PhD; Martin C. Stumpe, PhD; Derek Wu, BS; Subhashini Venugopalan, MS; Kasumi Widner, MS; Tom Madams, MEng; Jorge Cuadros, OD, PhD; R Rajiv Raman, MS, DNB; Philip C. Nelson, BS; Jessica L. Mega, MD, MPH; Dale R. Webster, PhD

IMPORTANCE Deep learning is a family of computational methods that allow an algo program itself by learning from a large set of examples that demonstrate the desired behavior, removing the need to specify rules explicitly. Application of these methods medical imaging requires further assessment and validation.

OBJECTIVE To apply deep learning to create an algorithm for automated detection o retinopathy and diabetic macular edema in retinal fundus photographs.

DESIGN AND SETTING A specific type of neural network optimized for image classific called a deep convolutional neural network was trained using a retrospective develo data set of 128 175 retinal images, which were graded 3 to 7 times for diabetic retino diabetic macular edema, and image gradability by a panel of 54 US licensed ophthal and ophthalmology senior residents between May and December 2015. The resulta algorithm was validated in January and February 2016 using 2 separate data sets, bo graded by at least 7 US board-certified ophthalmologists with high intragrader consi

Figure 3. Validation Set Performance for All-Cause Referable Diabetic Retinopathy in the EyePACS-1 Data Set (9946 Images)

Convolutional Neural Net

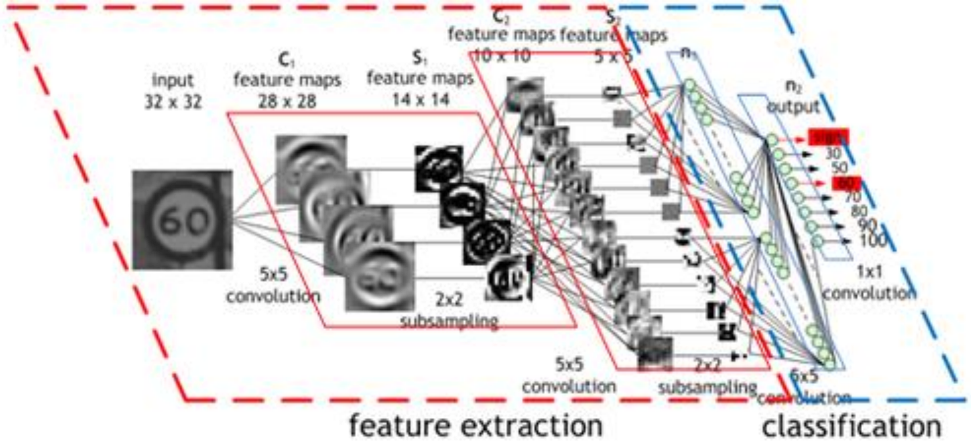

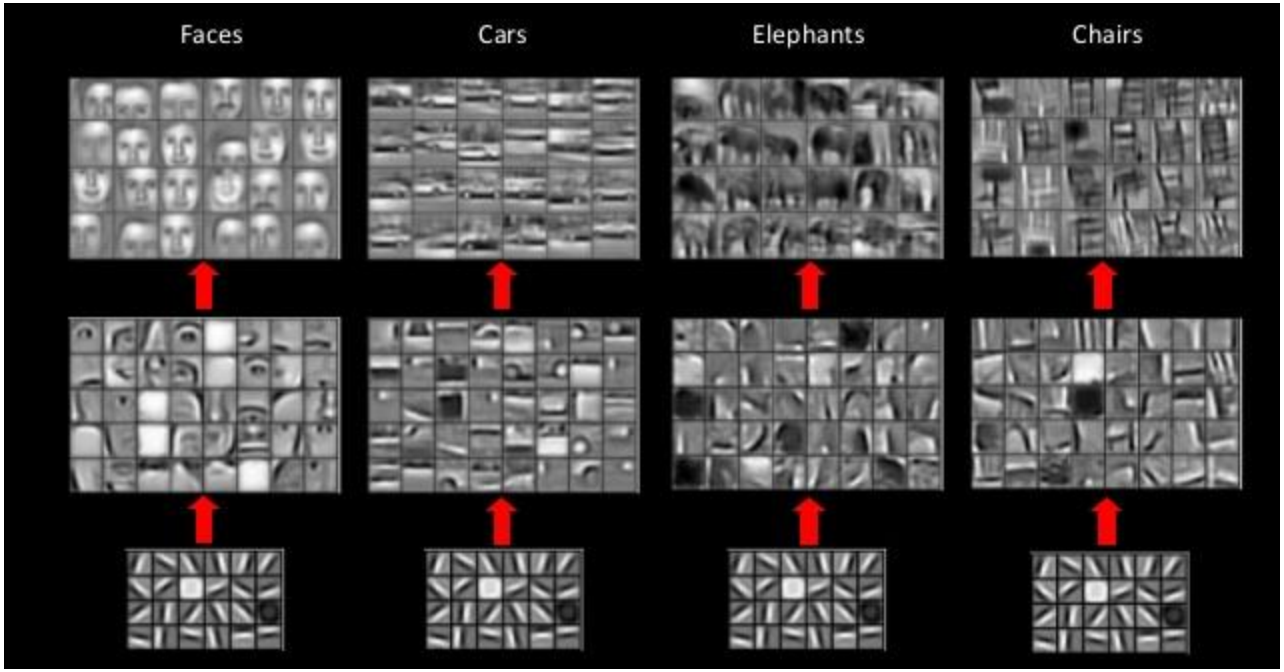

Convolutional Neural Net

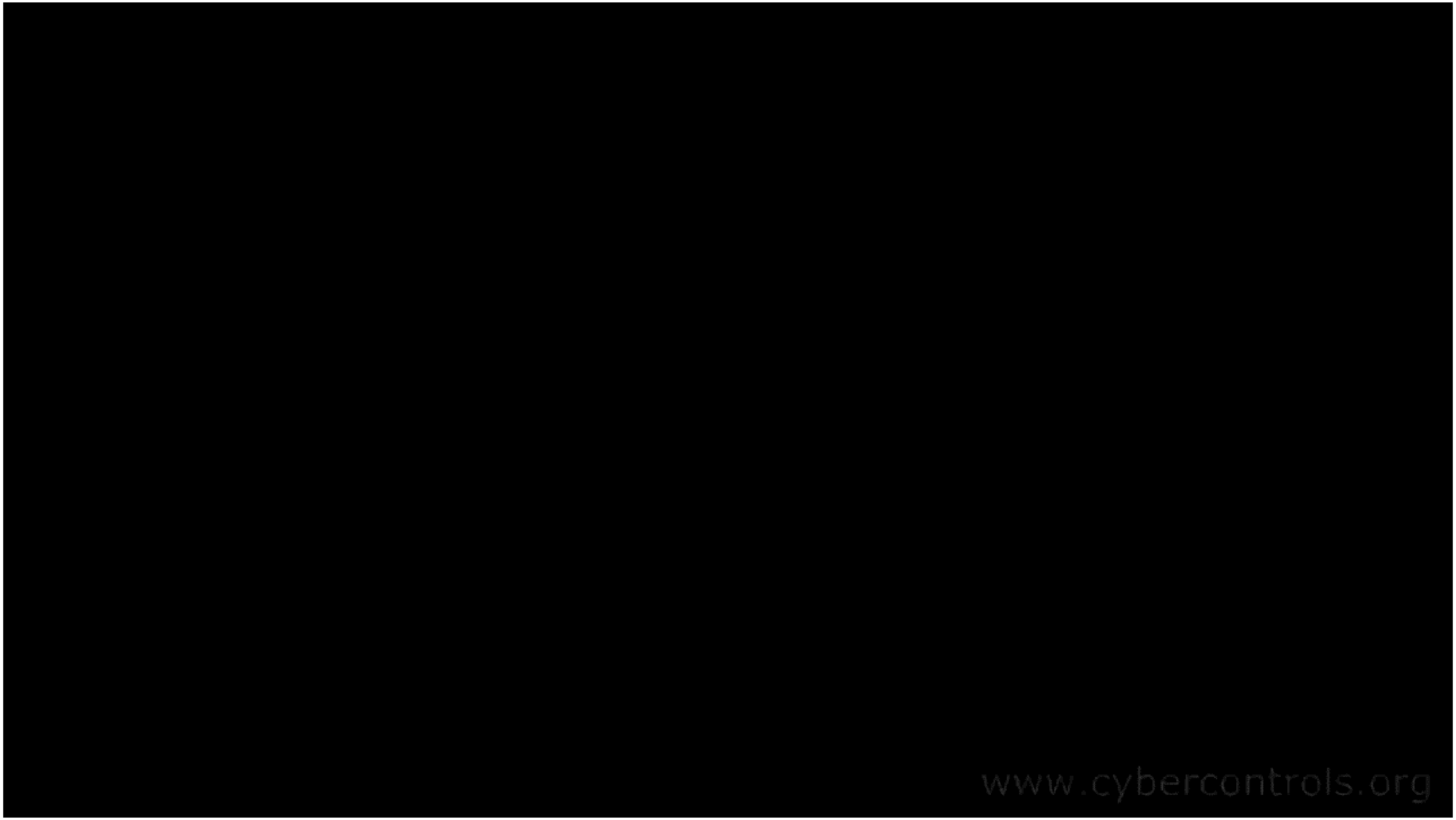

인공지능 기술의 혁신: 의료영상

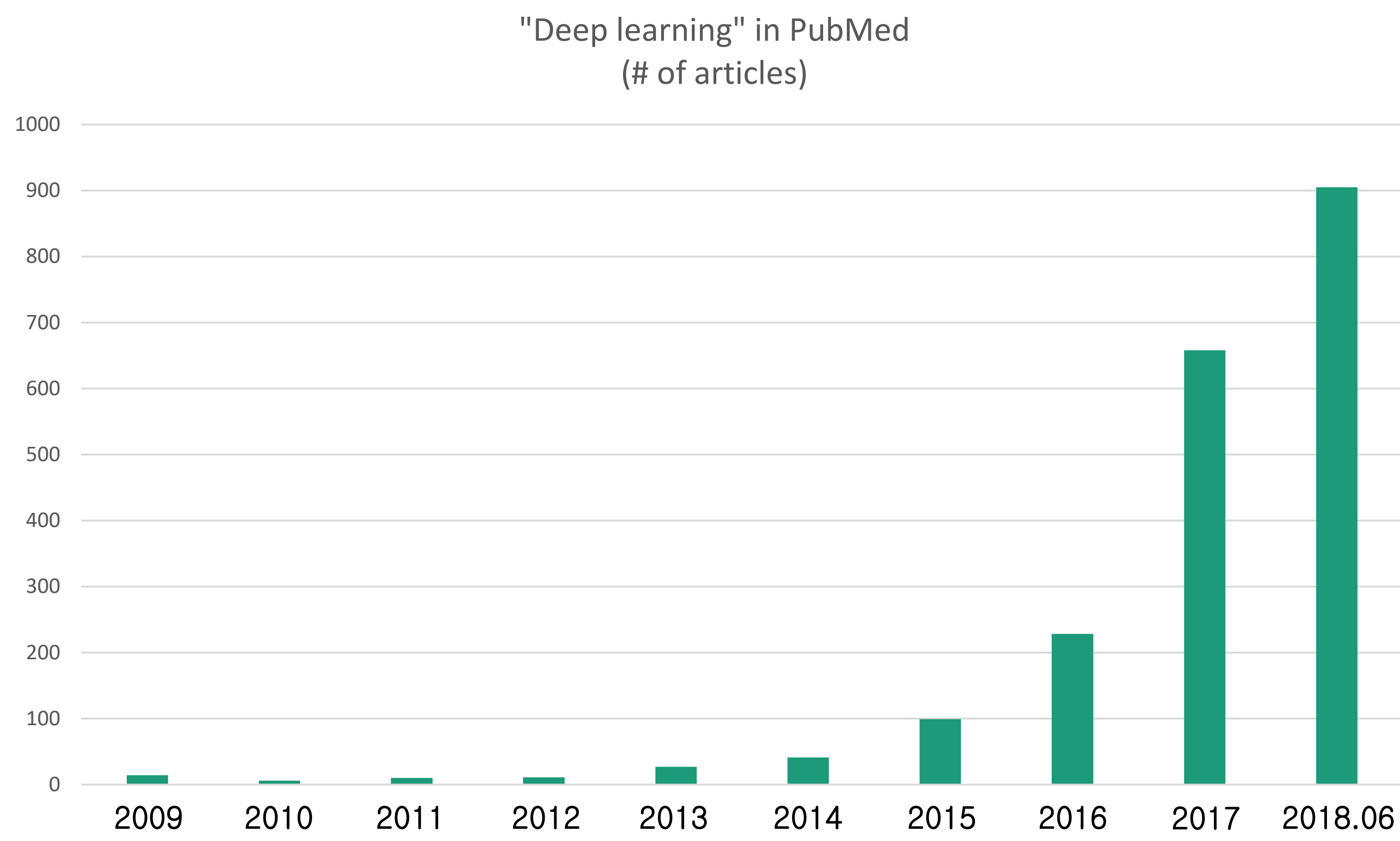

인공지능 기술의 혁신: 의료영상

Research

JAMA | Original Investigation | INNOVATIONS IN HEALTH CARE DELIVERY

Development and Validation of a Deep Learning Algorithm for Detection of Diabetic Retinopathy in Retinal Fundus Photographs

Varun Gulshan, PhD; Lily Peng, MD, PhD; Marc Coram, PhD; Martin C. Stumpe, PhD; Derek Wu, BS; Arunachalam Narayanaswamy, PhD; Subhashini Venugopalan, MS; Kasumi Widner, MS; Tom Madams, MEng; Jorge Cuadros, OD, PhD; Ramasamy Kim, OD, DNB; Rajiv Raman, MS, DNB; Philip C. Nelson, BS; Jessica L. Mega, MD, MPH; Dale R. Webster, PhD

IMPORTANCE program itself behavior, rem medical imagi

OBJECTIVE To retinopathy a

DESIGN AND S called a deep data set of 12 diabetic macu and ophthalm algorithm was graded by at l

EXPOSURE De

MAIN OUTCOM referable diab referable diab

LETTER

doi:10.1038/nature21056

Dermatologist-level classification of skin cancer with deep neural networks

Andre Esteva[1]*, Brett Kuprel[1]*, Roberto A. Novoa[2,3], Justin Ko[2], Susan M. Swetter[2,4], Helen M. Blau[5] & Sebastian Thrun[6]

Skin cancer, the most common human malignancy[1–3], is primarily diagnosed visually, beginning with an initial clinical screening and followed potentially by dermoscopic analysis, a biopsy and histopathological examination. Automated classification of skin

images (for example, smartphone images) exhibit variability in factors such as zoom, angle and lighting, making classification substantially more challenging[23,24]. We overcome this challenge by using a data-driven approach—1.41 million pre-training and training images

Research

JAMA | Original Investigation

Diagnostic Assessment of Deep Learning Algorithms for Detection of Lymph Node Metastases in Women With Breast Cancer

Babak Ehteshami Bejnordi, MS; Mitko Veta, PhD; Paul Johannes van Diest, MD, PhD; Bram van Ginneken, PhD; Nico Karssemeijer, PhD; Geert Litjens, PhD; Jeroen A. W. M. van der Laak, PhD; and the CAMELYON16 Consortium

ChosunBiz
2018. 6. 23 (토)

뉴스 | 증권 | 부동산 | 정책·금융 | 기업 | 오피니언

기업 ▾
바이오·제약

인공지능(AI)으로 뼈 나이 판독...식약처, 뷰노 개발 의료기기 첫 판매 허가

허지윤 기자 ▾

기사 | 100자평(0) | +크게 | −작게

입력 : 2018.05.16 11:11

의료현장에서 인공지능 기술을 활용해 뼈(骨) 나이를 판독할 수 있게 됐다. 규제당국이 국내에서 개발한 인공지능(AI) 기반 의료기기 판매를 처음으로 허가했다.

식품의약품안전처는 국내 의료기기업체 '뷰노'가 개발한 인공지능(AI) 기술이 적용된 의료영상분석장치소프트웨어 '뷰노메드 본에이지(VUNOmed-BoneAge)'를 16일 허가했다고 밝혔다.

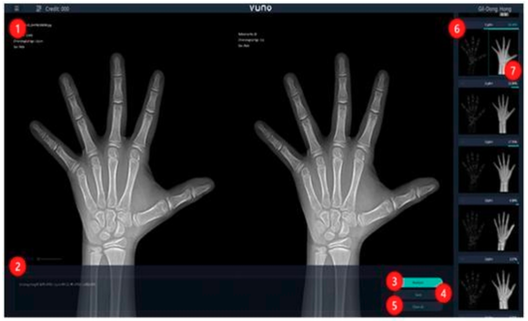

▲ 뷰노의 AI기반 의료영상분석장치 소프트웨어 '뷰노메드 본에이지(VUNOmed-BoneAge)', /식약처 제공

Beyond computer vision

Computer Vision
To Discern
Clinician Behaviors

"Bedside Computer Vision"

Yeung S, Fei-Fei Li et al. NEJM 2018 April

Brain

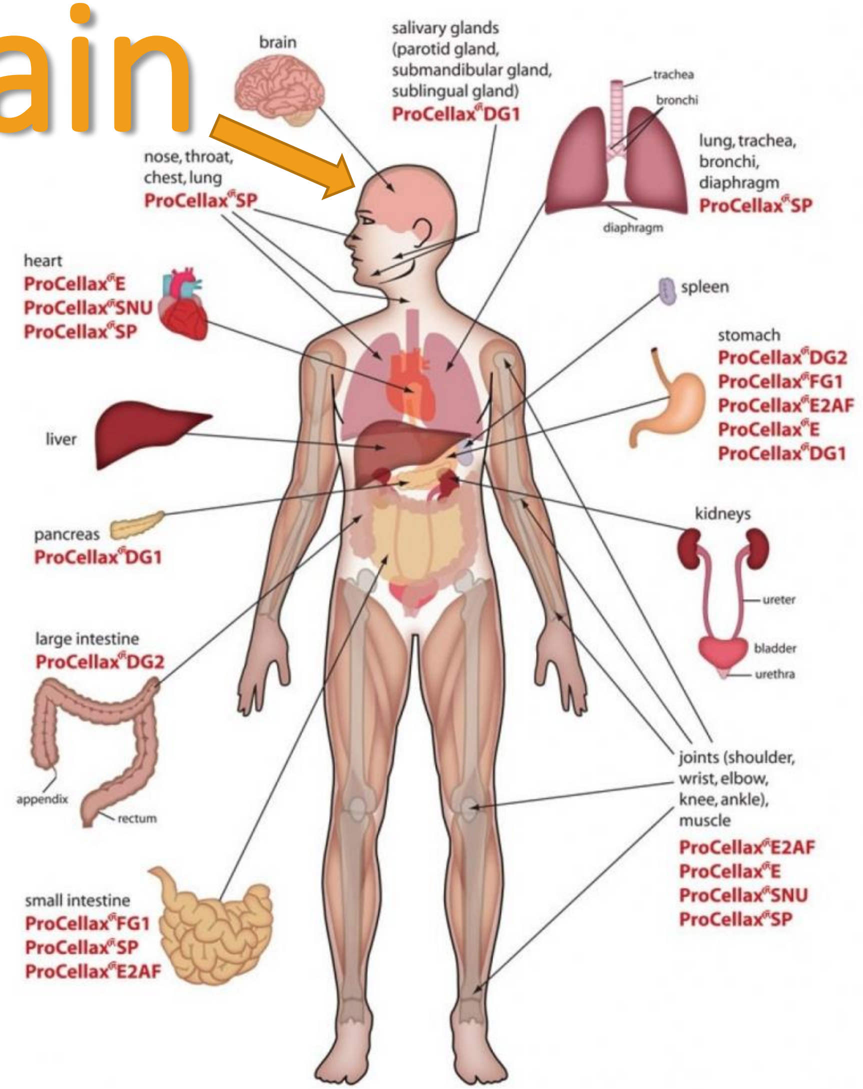

brain
salivary glands (parotid gland, submandibular gland, sublingual gland)
ProCellax®DG1
trachea
bronchi
lung, trachea, bronchi, diaphragm
ProCellax®SP
diaphragm
nose, throat, chest, lung
ProCellax®SP
heart
ProCellax®E
ProCellax®SNU
ProCellax®SP
spleen
stomach
ProCellax®DG2
ProCellax®FG1
ProCellax®E2AF
ProCellax®E
ProCellax®DG1
liver
kidneys
ureter
bladder
urethra
pancreas
ProCellax®DG1
large intestine
ProCellax®DG2
appendix
rectum
joints (shoulder, wrist, elbow, knee, ankle), muscle
ProCellax®E2AF
ProCellax®E
ProCellax®SNU
ProCellax®SP
small intestine
ProCellax®FG1
ProCellax®SP
ProCellax®E2AF

Tumor

- Segmentation of Glioblastoma Malformation (GBM)
  - Multi-class segmentation
    - ✓ Necrosis
    - ✓ Enhancing tumor
    - ✓ Edema
  - AMC dataset
    - ✓ 103 patients
    - ✓ 3D enhanced-T1w

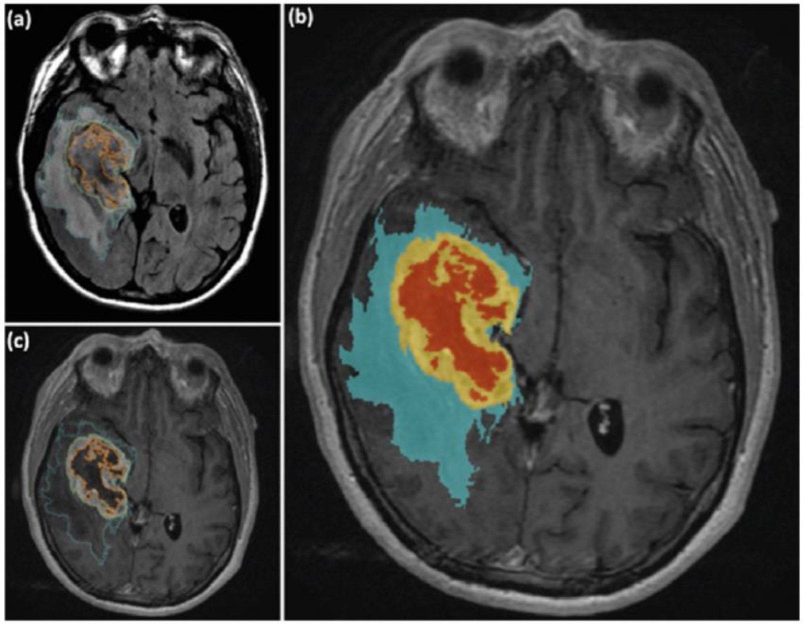

Tumor

- Segmentation of Glioblastoma Malformation (GBM)
  - Phase 1: localization (coarse segmentation)

Data dividing to 8 cube

1. Image & Mask cropping

size
448 x 448 x 224
512 x 512 x 256
➡ 352 x 416 x 192

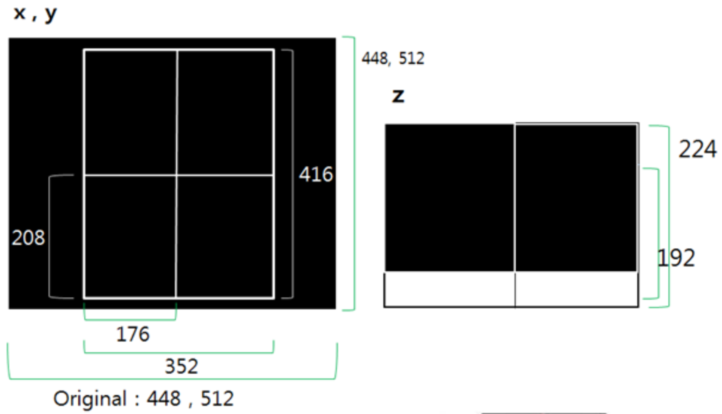

	Label	Set
T1ce	Enhanced	Train 600 Valid 112 Test 112
	Enhanced +Necrosis	Train 600 Valid 112 Test 112

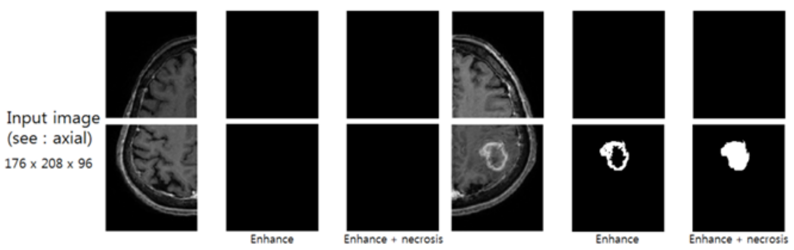

2. Divided to 8 cube

size
352 x 416 x 192
➡ 176 x 208 x 96

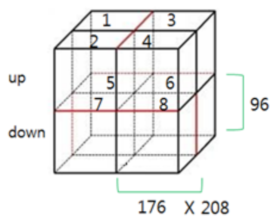

3D U-net Training

Input

one of the most widely used CNN architectures for image segmentation

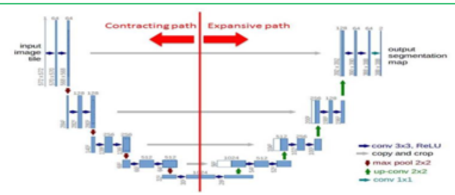

Tumor

- Segmentation of Glioblastoma Malformation (GBM)
  - Phase 2: fine segmentation

Data augmentation (Method : Random Cropping)

Random cropping on the masks were performed

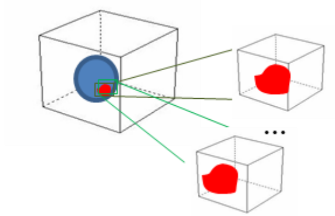

Image

Mask

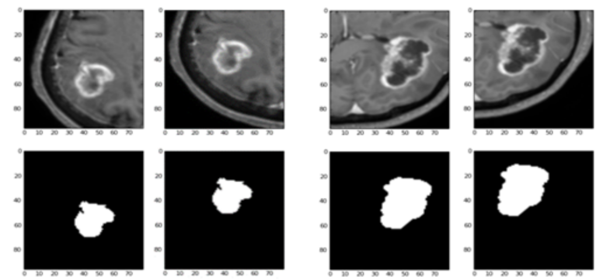

Data set

(unit : subject)

Num of Random crop	Train	Valid	Test
1	62	20	21
2	124	40	21
4	256	80	21
8	496	160	21

Input

3D U-net Training

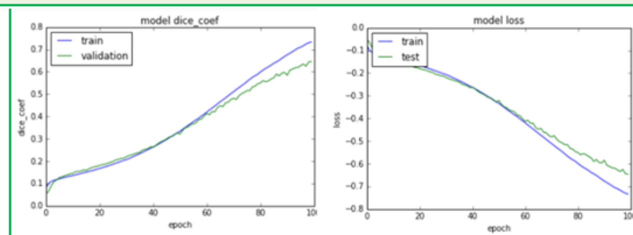

Tumor

- Segmentation of Glioblastoma Malformation (GBM)
  - Results

Enhancing	Dice	Jaccard
coarse	0.819	0.701
x1	0.648	0.511
x2	0.707	0.567
x4	0.771	0.642
x8	0.823	0.711
x16	0.834	0.725

Necrosis	Dice	Jaccard
coarse	0.788	0.684
x1	0.445	0.324
x2	0.641	0.517
x4	0.717	0.594
x8	0.778	0.658
x16	0.848	0.759

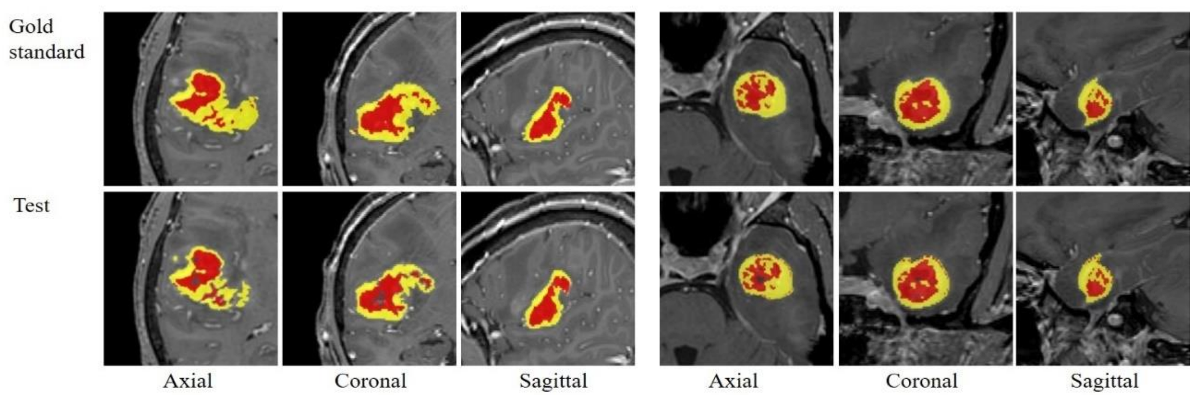

Tumor

- Classification
  - Binary classification: PCNSL vs. GBM

PCNSL (primary CNS lymphoma)

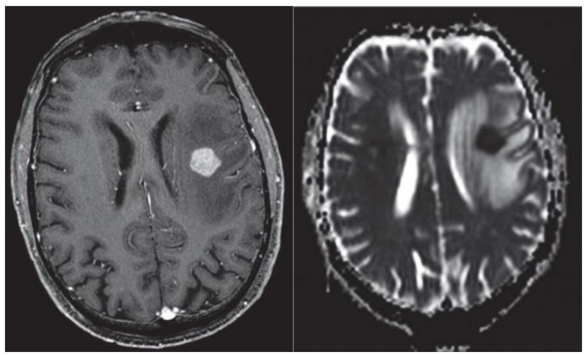

T1CE ADC

vs.

GBM(glioblastoma)

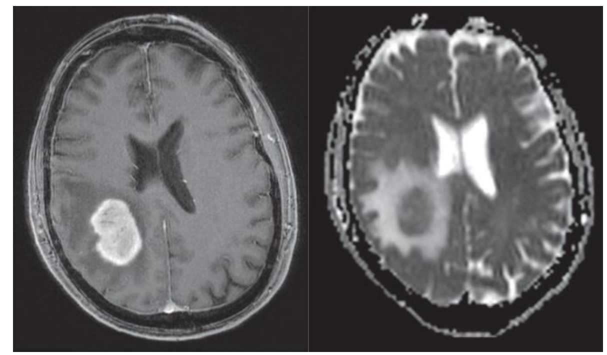

T1CE ADC

  - Multi-center: AMC and Samsung Medical Center

	ASAN Medical Center		Samsung Medical Center	
Pathology	PCNSL	GBM	PCNSL	GBM
Patients (N)	62	91	14	28

	Training		Internal validation	
Pathology	PCNSL	GBM	PCNSL	GBM
Patients (N)	50	73	12	18

Tumor

- Classification
  - Binary classification: PCNSL vs. GBM

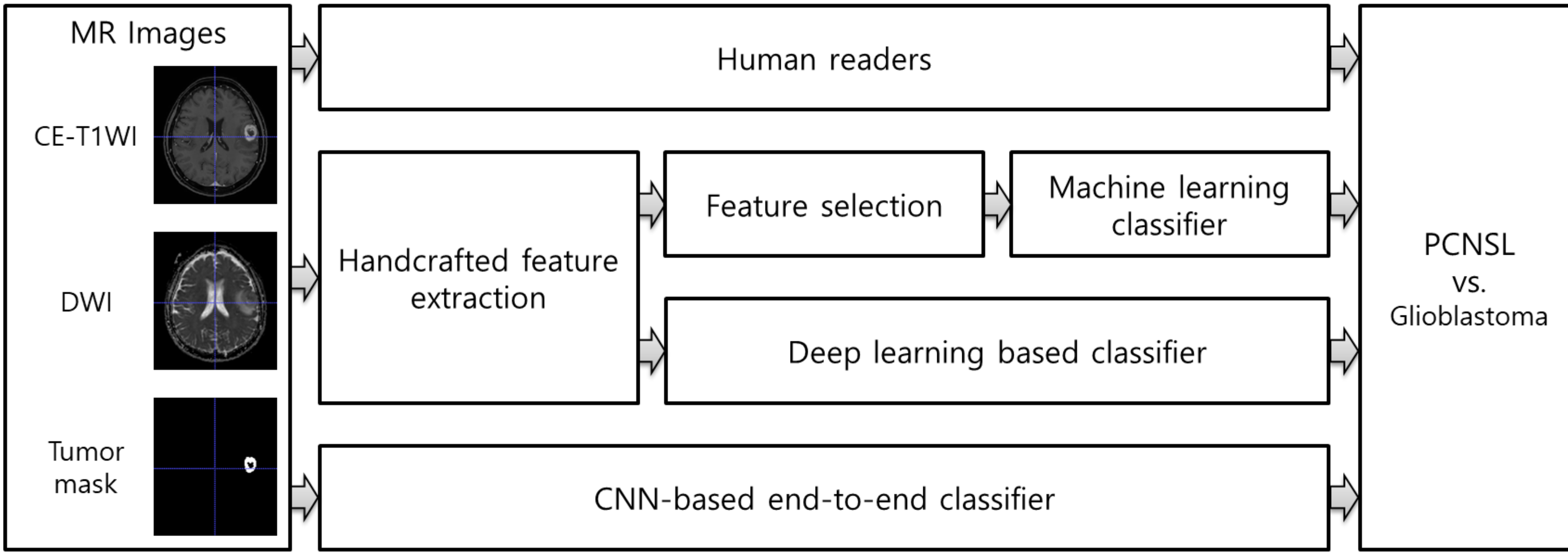

Tumor

- Classification
  - Pre-processing
    - ✓ Bias correction
    - ✓ Intensity normalization
  - Handcrafted features
    - ✓ First order: 17
    - ✓ GLCM (dist=1,2,3): 25x3 = 75
    - ✓ GLRLM: 12

    104 features

    × 9 wavelets (original + 8 wavelets) = 936 features

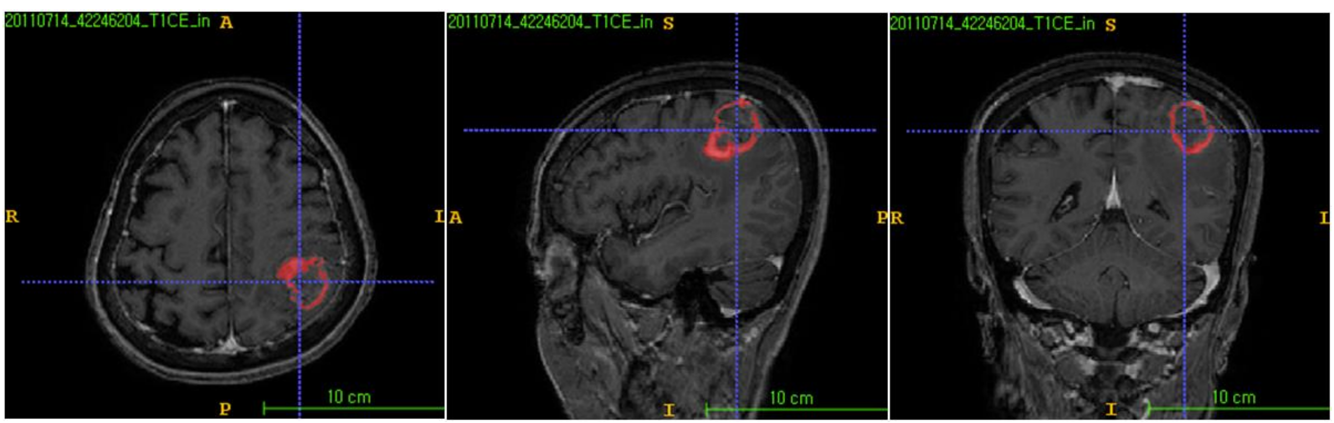

Tumor

- Classification
  - Results: Handcrafted features + NN

Network	Data	Internal validation				External validation (z-scoring with training dataset)				External validation (z-scoring with test dataset)			
		AUC (95% CI)	Acc. (%)	Sen. (%)	Spec. (%)	AUC (95% CI)	Acc. (%)	Sen. (%)	Spec. (%)	AUC (95% CI)	Acc. (%)	Sen. (%)	Spec. (%)
100-10	T1	0.9652 (0.9589, 0.9715)	93.33	91.67	94.44	0.9179 (0.9137, 0.9221)	83.33	78.57	85.71	0.9107 (0.9067, 0.9147)	85.71	85.71	85.71
	ADC	0.9692 (0.9603, 0.9781)	93.33	91.67	94.44	0.8598 (0.8351, 0.8845)	80.95	92.86	75.00	0.8426 (0.8254, 0.8598)	78.57	64.29	85.71
	T1 +ADC	0.9907 (0.9869, 0.9945)	100	100	100	0.9466 (0.9372, 0.9560)	85.71	92.86	82.14	0.9503 (0.9448, 0.9558)	85.71	92.86	82.14
500-100-10	T1	0.9655 (0.9602, 0.9708)	86.67	91.67	83.33	0.9152 (0.9081, 0.9223)	83.33	78.57	85.71	0.9100 (0.9042, 0.9158)	83.33	78.57	85.71
	ADC	0.9680 (0.9566, 0.9794)	93.33	91.67	94.44	0.8366 (0.8109, 0.8623)	73.81	100	60.71	0.8428 (0.8278, 0.8578)	76.19	64.29	82.14
	T1 +ADC	0.9903 (0.9873, 0.9933)	100	100	100	0.9345 (0.9245, 0.9445)	85.71	92.86	82.14	0.9480 (0.9412, 0.9548)	83.33	85.71	82.14
500-100-50-10	T1	0.9556 (0.9493, 0.9619)	86.67	91.67	83.33	0.9101 (0.9022, 0.9180)	83.33	78.57	85.71	0.9103 (0.9048, 0.9158)	83.33	78.57	85.71
	ADC	0.9638 (0.9526, 0.9750)	93.33	91.67	94.44	0.8342 (0.8084, 0.8600)	80.95	92.86	75.00	0.8359 (0.8194, 0.8524)	76.19	64.29	82.14
	T1 +ADC	0.9893 (0.9853, 0.9933)	100	100	100	0.9245 (0.9163, 0.9327)	85.71	92.86	82.14	0.9418 (0.9328, 0.9508)	85.71	92.86	82.14

Tumor

▪ Classification

- Results: CNN-based end-to-end

	Data	Internal validation				External validation			
		AUC (95% CI)	Acc. (%)	Sen. (%)	Spec. (%)	AUC (95% CI)	Acc. (%)	Sen. (%)	Spec. (%)
Inception v3 (without data augmentation)	T1CE	0.8197 (0.7881, 0.8513)	73.33	41.67	94.44	0.5091 (0.4945, 0.5237)	42.86	57.14	35.71
	ADC	0.8794 (0.8568, 0.9020)	83.33	83.33	83.33	0.4857 (0.4687, 0.5027)	35.71	100	3.57
	T1CE+ADC	0.7945 (0.7719, 0.8171)	76.67	41.67	100	0.6019 (0.5845, 0.6193)	40.48	50.00	35.71

Stroke

- Infarct segmentation with SE block
  - Squeeze-and-Excitation Block

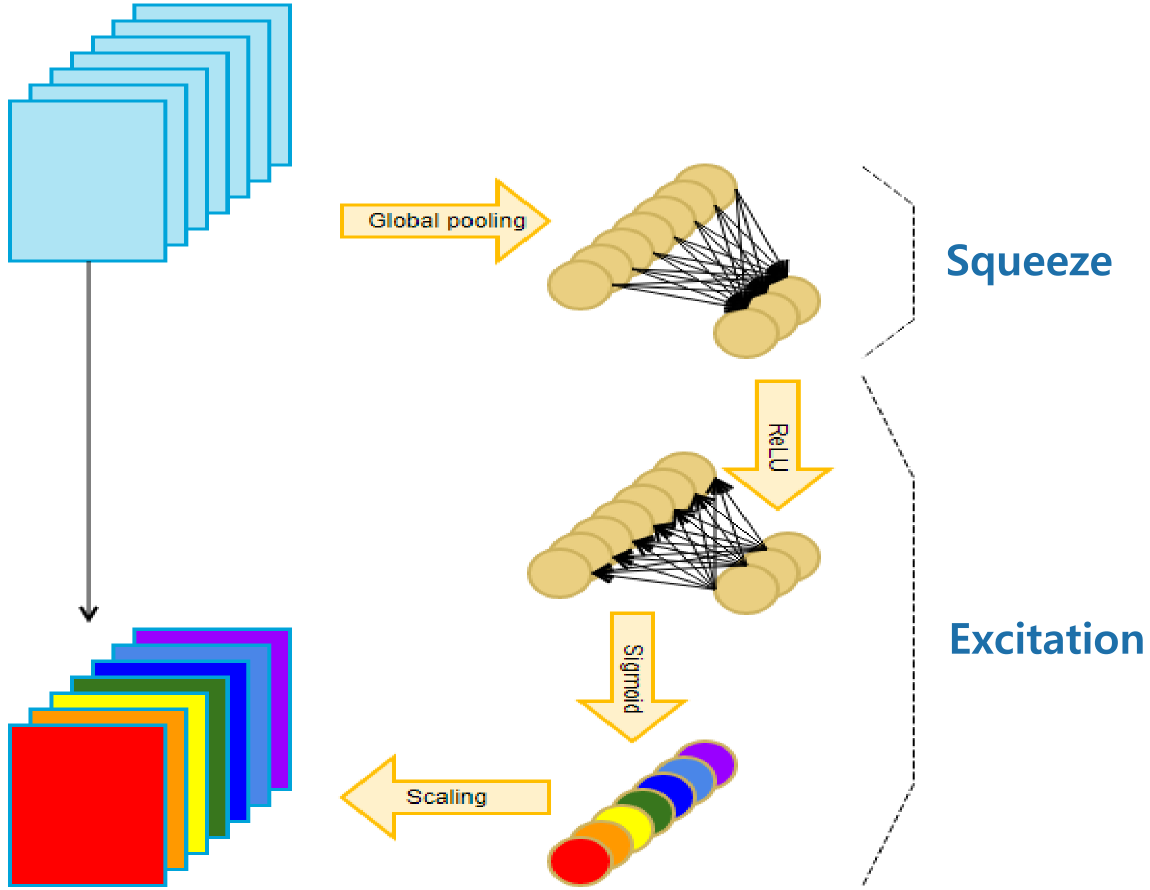

Stroke

- Infarct segmentation with SE block
  - Networks: U-net and Dense-net

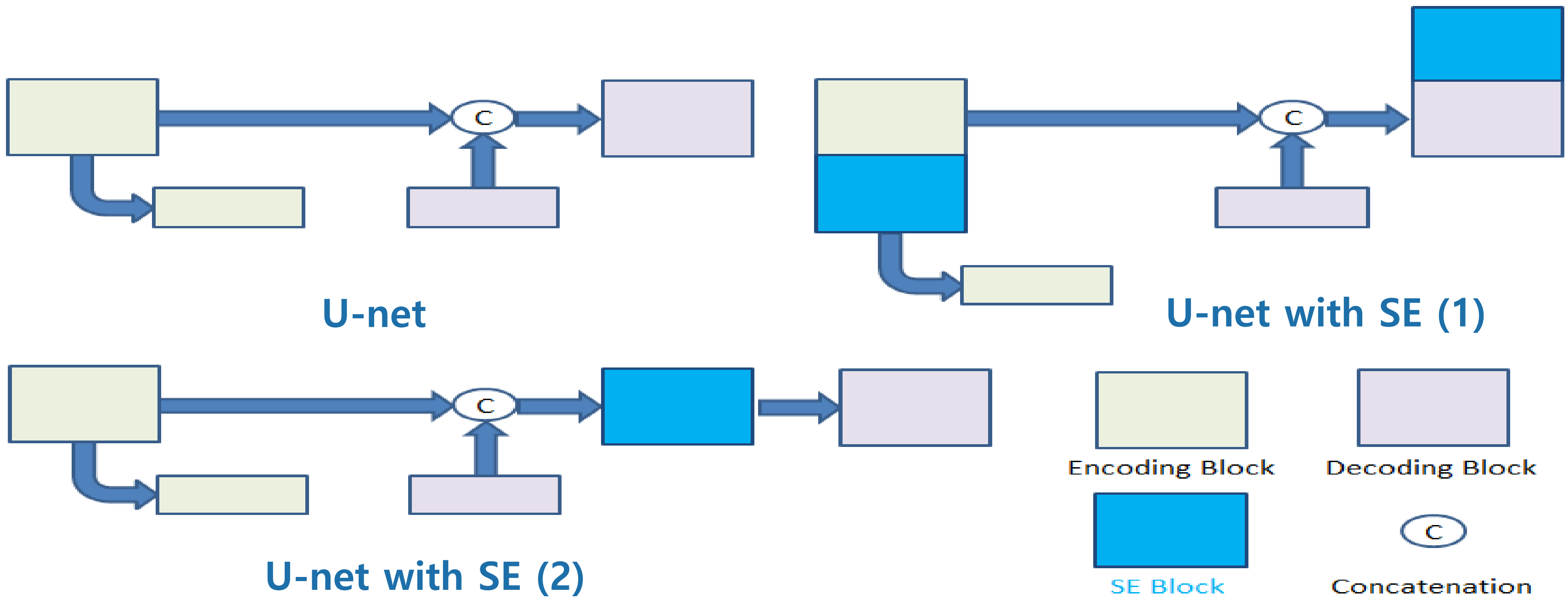

Stroke

- Infarct segmentation with SE block
  - Networks: U-net and Dense-net

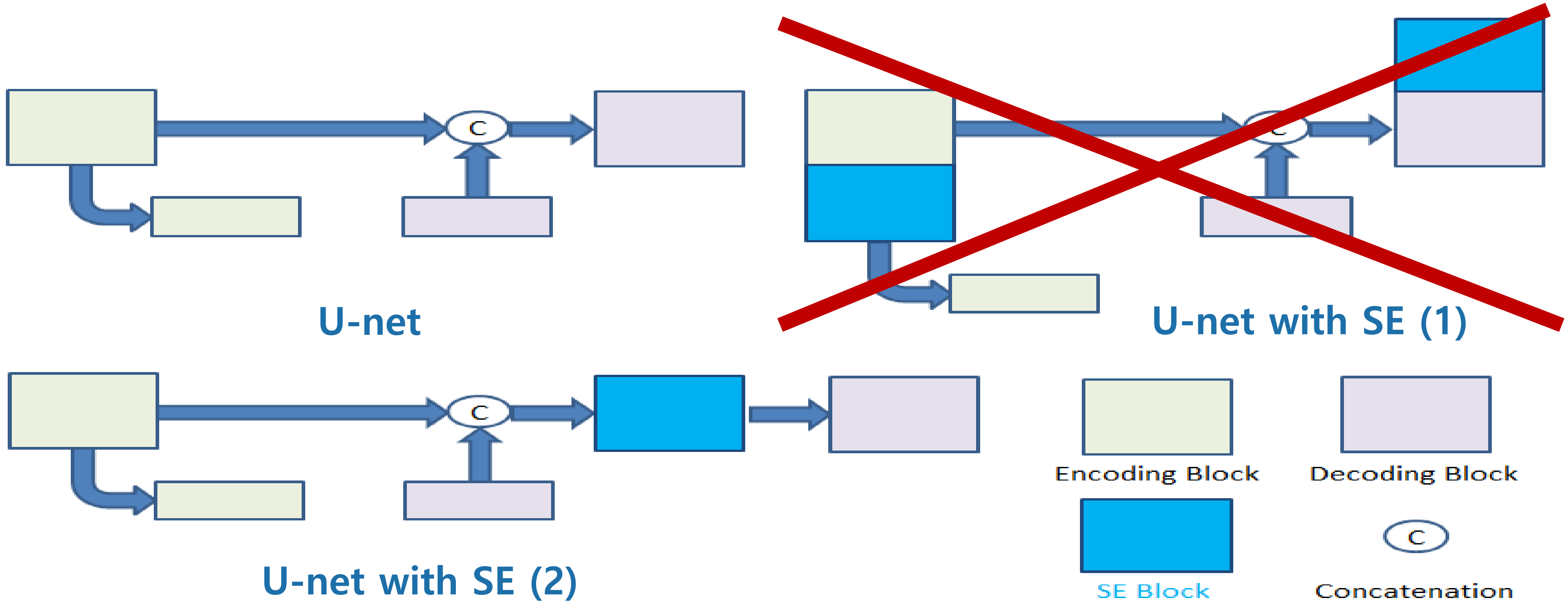

Stroke

- Infarct segmentation with SE block
  - Networks: U-net and Dense-net

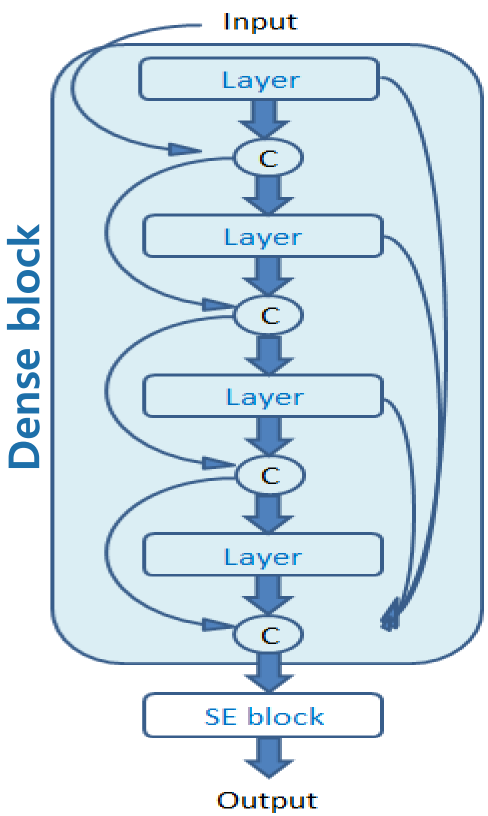

SE-dense block

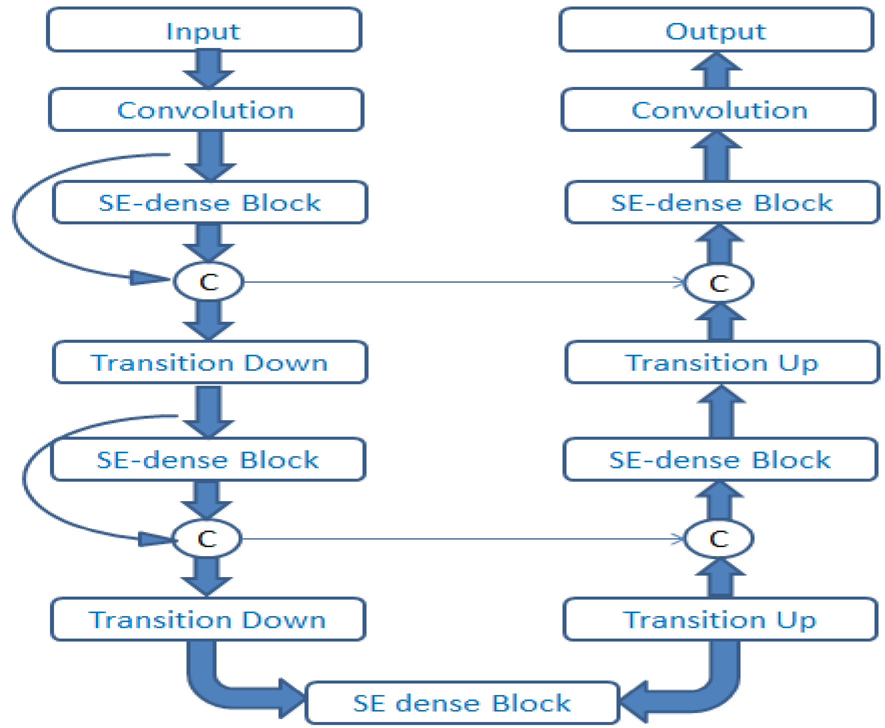

Dense-net with SE

Stroke

- Infarct segmentation with SE block
  - AMC dataset
    - ✓ 436 acute stroke patients
    - ✓ DWI scans: b1000 and ADC
  - Pre-processing
    - ✓ Resized volume size: 384 x 384 x 20
    - ✓ Fixed pixel spacing: 0.6510 mm x 0.6510 mm x 6.9 mm
    - ✓ Intensity normalization

Stroke

- Infarct segmentation with SE block
  - Results

Original	Dice	Jaccard	With SE	Dice	Jaccard
2D En-/De-coder	0.749	0.617	2D En-/De-coder	0.768	0.640
2D U-net	0.823	0.713	2D U-net	0.832	0.723
2D Dense-net	0.809	0.694	2D Dense-net	0.820	0.711
3D FCN	0.632	0.494	3D FCN	0.612	0.477
3D U-net	0.764	0.639	3D U-net	0.743	0.615

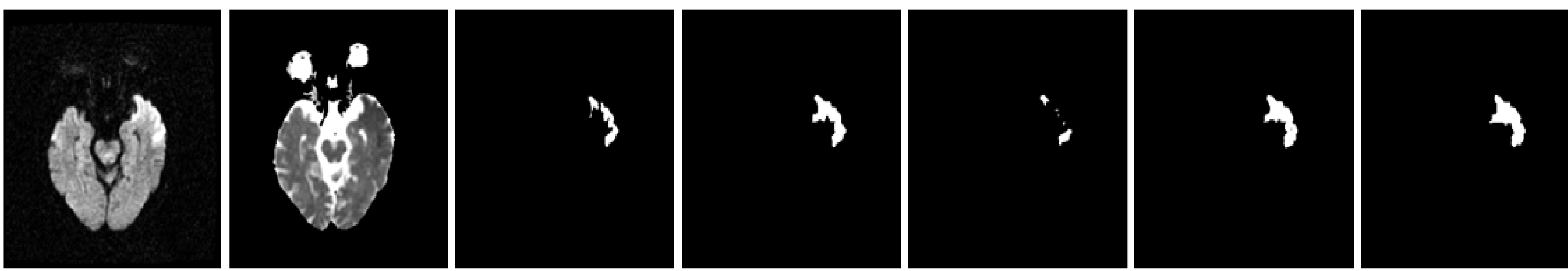

b1000 | ADC | Dense-net | Dense-net with SE | U-net | U-net with SE | GT

Chest

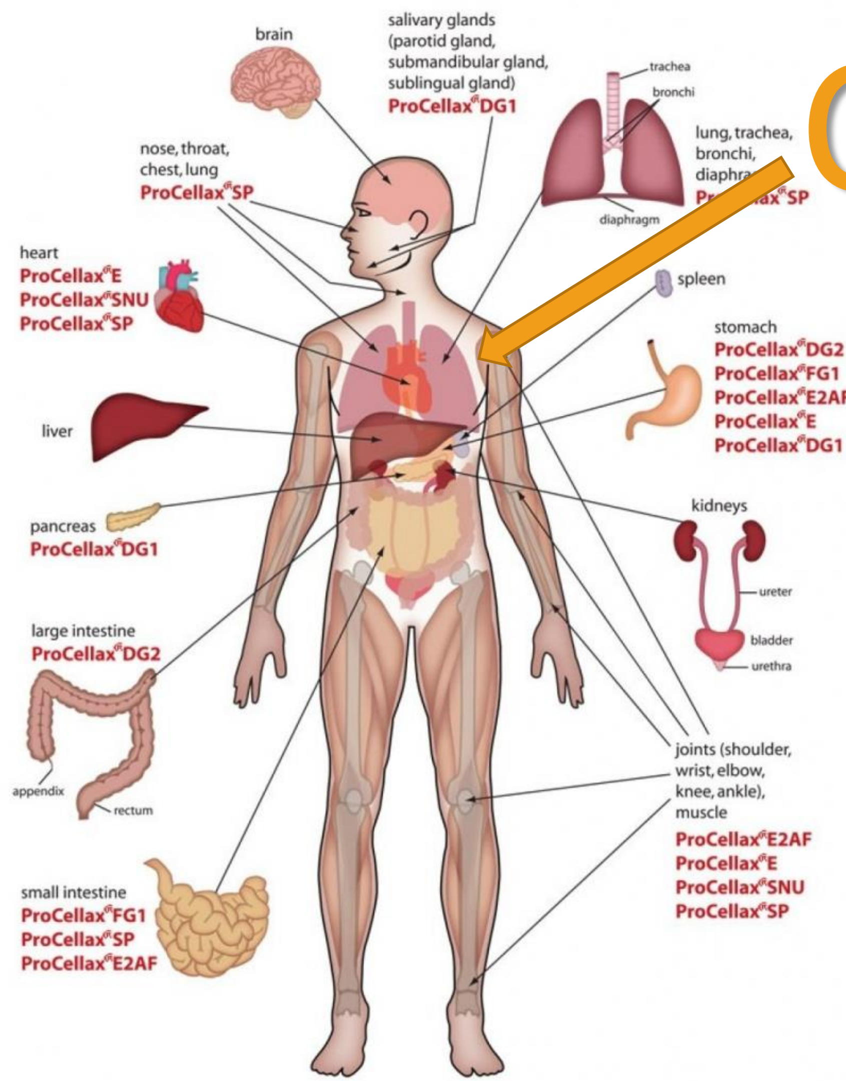

brain
salivary glands (parotid gland, submandibular gland, sublingual gland)
ProCellax®DG1
trachea
bronchi
lung, trachea, bronchi,
diaphragm
nose, throat, chest, lung
ProCellax®SP
heart
ProCellax®E
ProCellax®SNU
ProCellax®SP
spleen
stomach
ProCellax®DG2
ProCellax®FG1
ProCellax®E2AF
ProCellax®E
ProCellax®DG1
liver
kidneys
ureter
bladder
urethra
pancreas
ProCellax®DG1
large intestine
ProCellax®DG2
appendix
rectum
joints (shoulder, wrist, elbow, knee, ankle), muscle
ProCellax®E2AF
ProCellax®E
ProCellax®SNU
ProCellax®SP
small intestine
ProCellax®FG1
ProCellax®SP
ProCellax®E2AF

Chest PA: Curriculum learning

- Curriculum learning for multi-label classification
  - 5-label classification

Abnormal Screening
- classification

Annotation
- localization
- detection

Nodule
Consolidation
Interstitial opacity
Pleural effusion
Pneumothorax

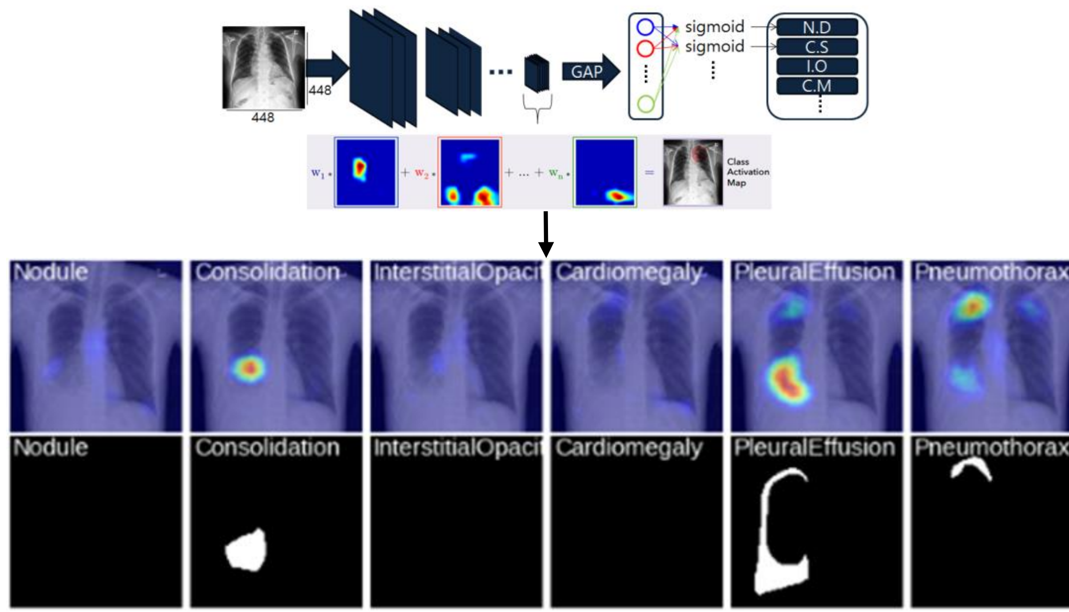

Chest PA: Curriculum learning

- Curriculum learning for multi-label classification
  - **Multi-class** classification
    - ✓ Each instance **exclusively** belong to **single class**

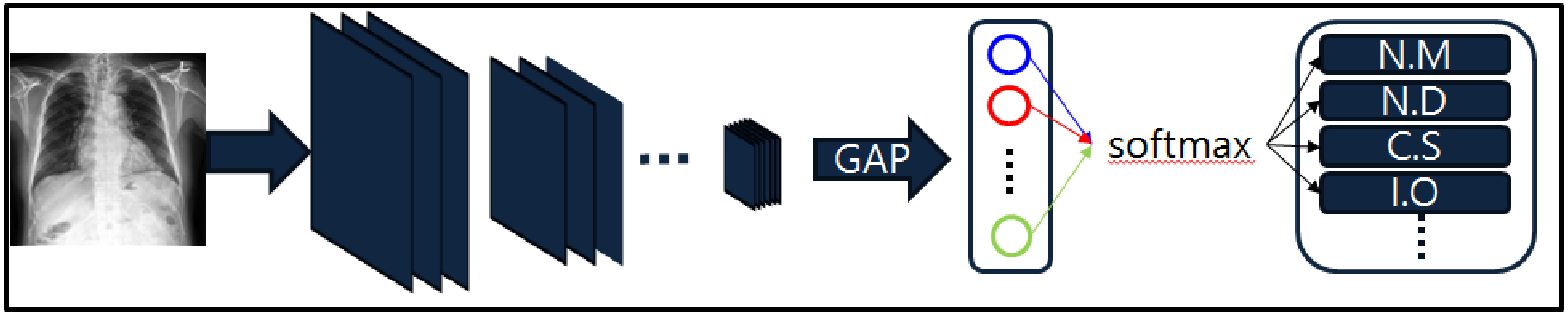

  - **Multi-label** classification
    - ✓ Each instance can belong to **multiple classes**

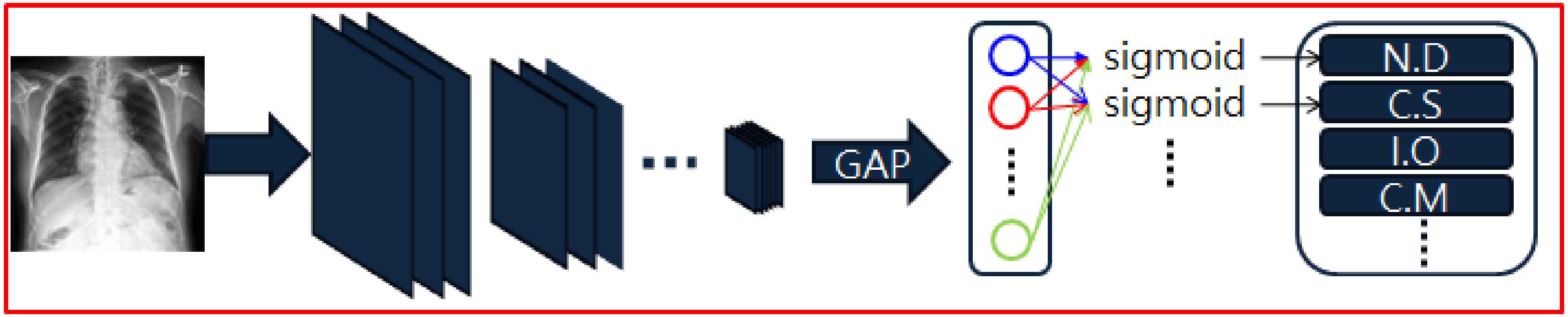

Chest PA: Curriculum learning

- Curriculum learning for multi-label classification
  - Curriculum learning: from patch to entire image

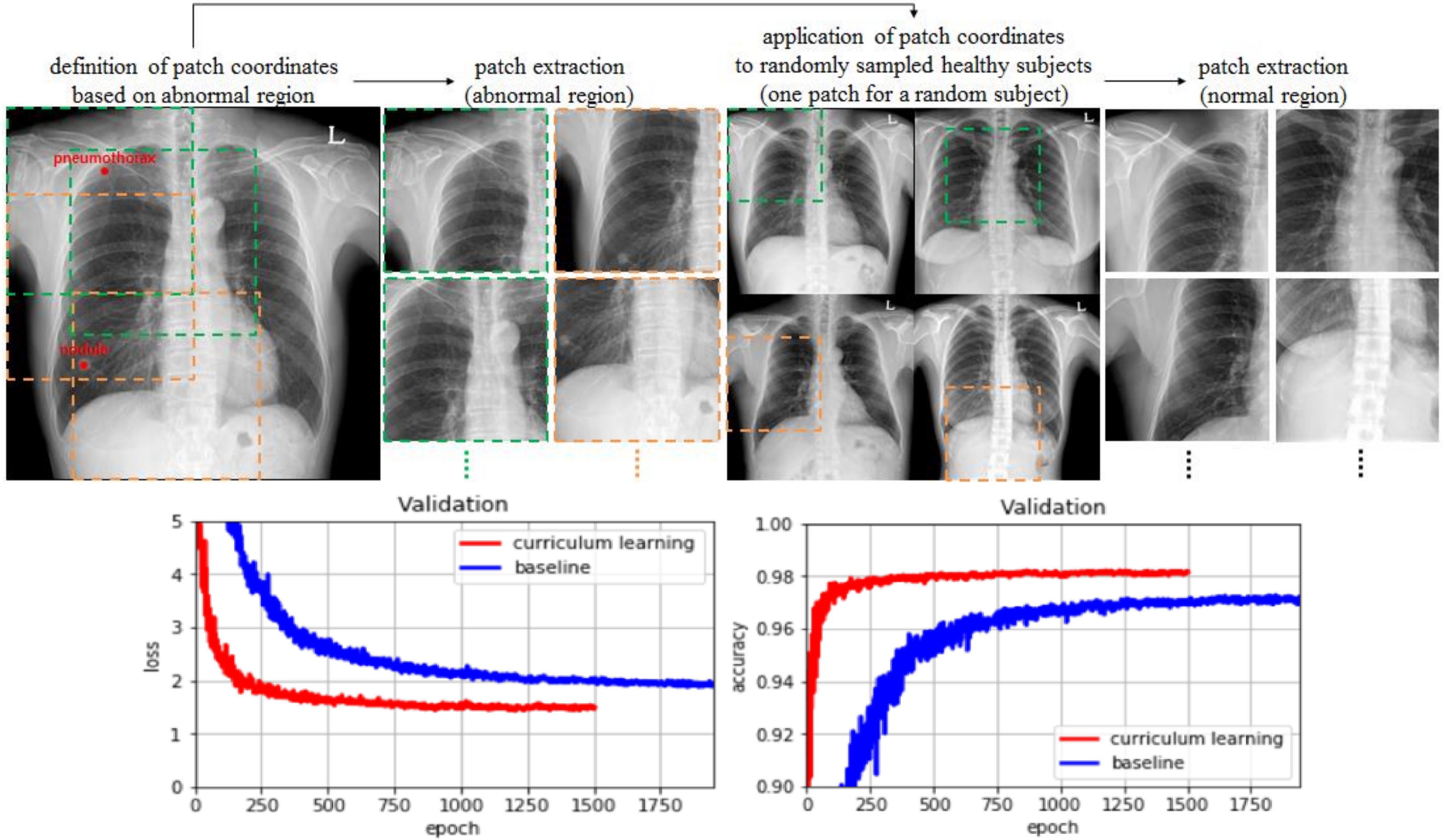

Chest PA: Curriculum learning

- Curriculum learning for multi-label classification
  - Results

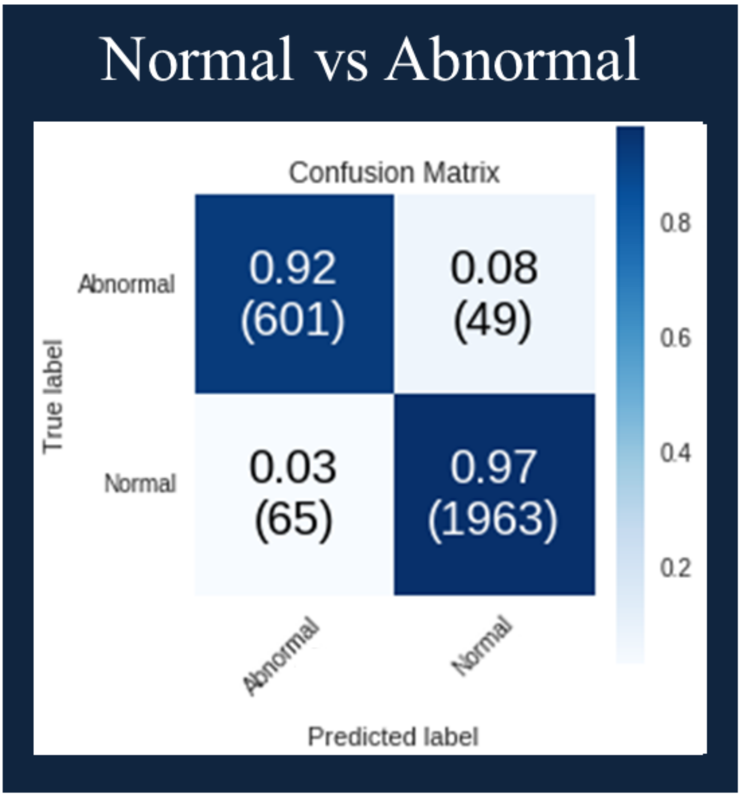

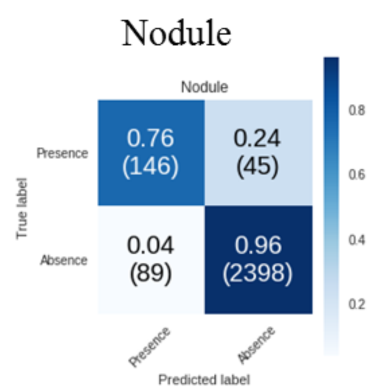

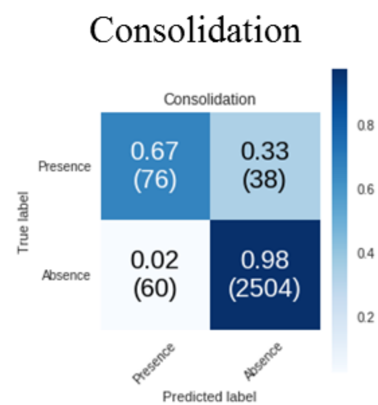

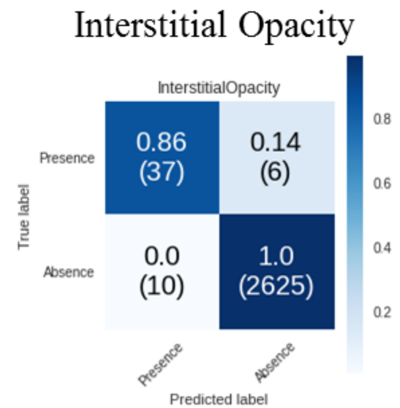

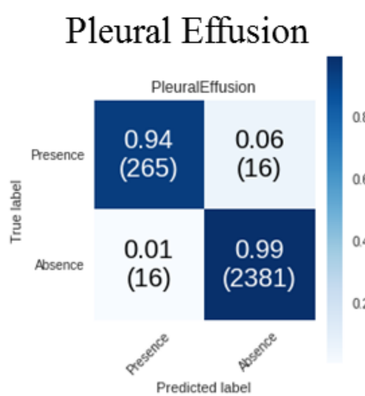

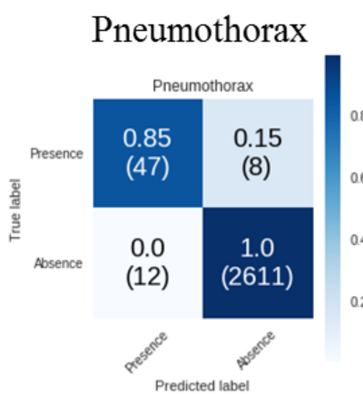

Chest PA: Curriculum learning

- Curriculum learning for multi-label classification
  - Results

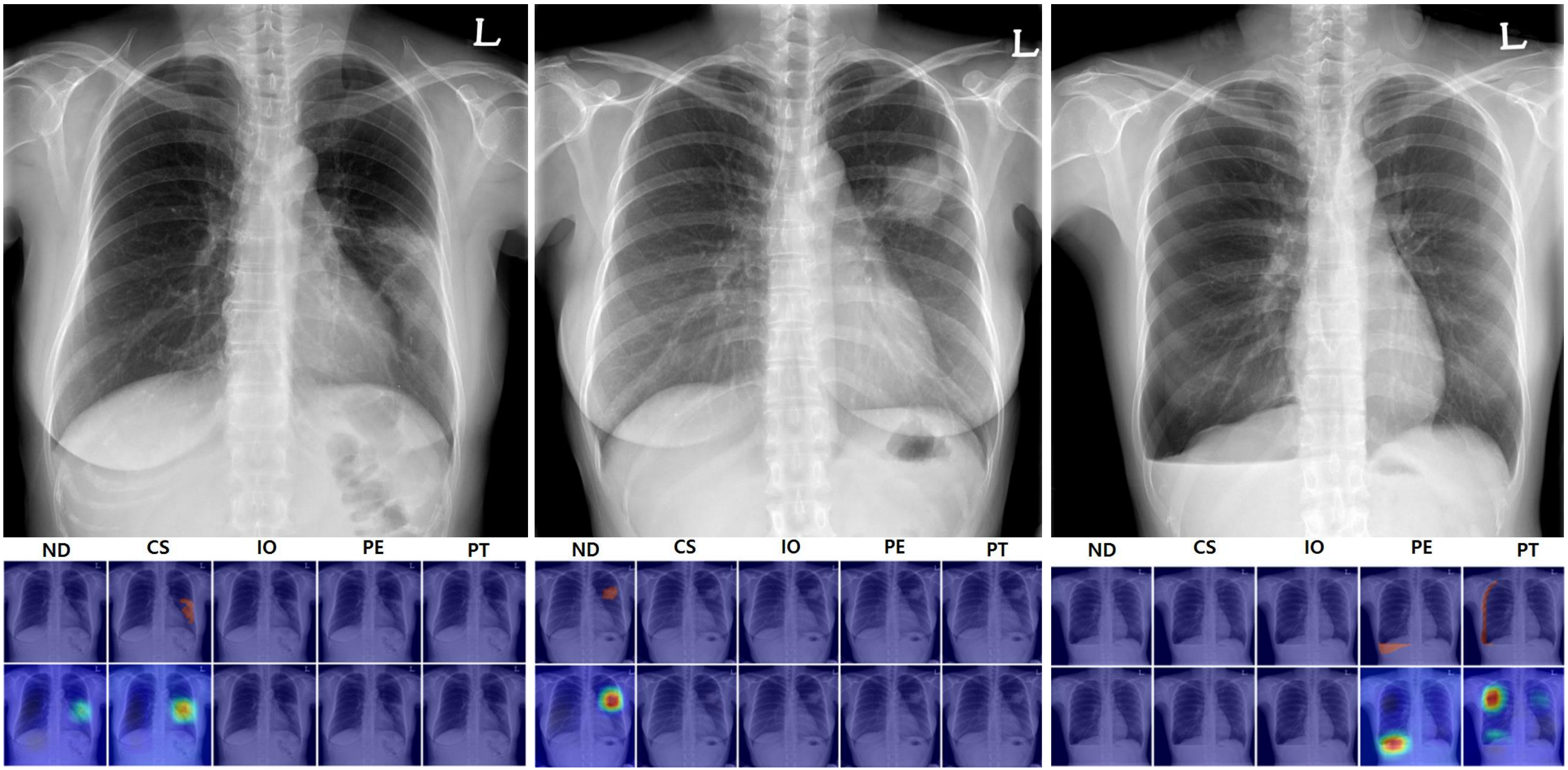

Chest PA: Reproducibility

- Reproducibility analysis on CNN-based detection
  - Using image pairs within short-term period (7 days)
  - 5-class detection
    - ✓ Nodule
    - ✓ Consolidation
    - ✓ Interstitial Opacity
    - ✓ Pleural Effusion
    - ✓ Pneumothorax
  - Network: YOLO v2

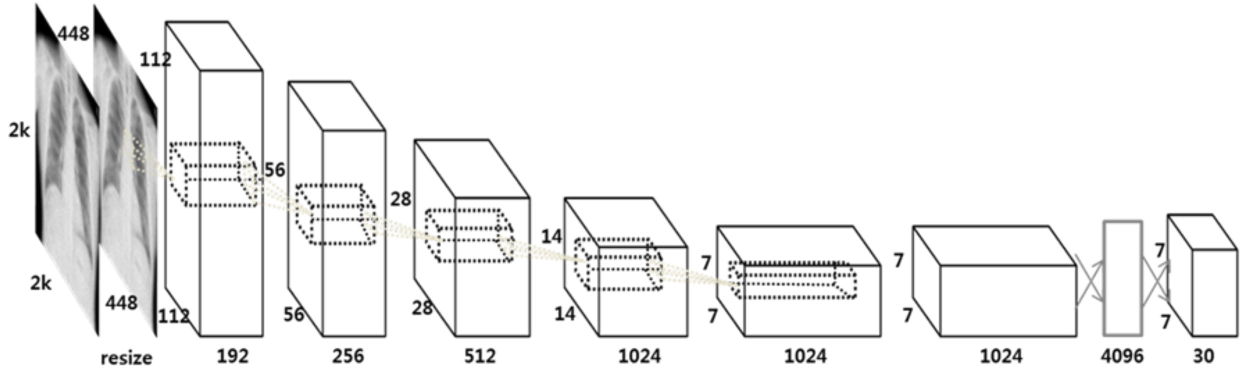

Chest PA: Reproducibility

- Reproducibility analysis on CNN-based detection
  - Results

Nodule (N = 121)		1st P	1st N
2nd	P	90	3
	N	19	8

Consol. (N = 27)		1st P	1st N
2nd	P	19	1
	N	4	4

I. O. (N = 12)		1st P	1st N
2nd	P	12	0
	N	0	0

P. E. (N = 67)		1st P	1st N
2nd	P	61	0
	N	2	4

Pneumotho. (N = 21)		1st P	1st N
2nd	P	13	1
	N	2	4

Chest PA: Reproducibility

- Reproducibility analysis on CNN-based detection
  - Results

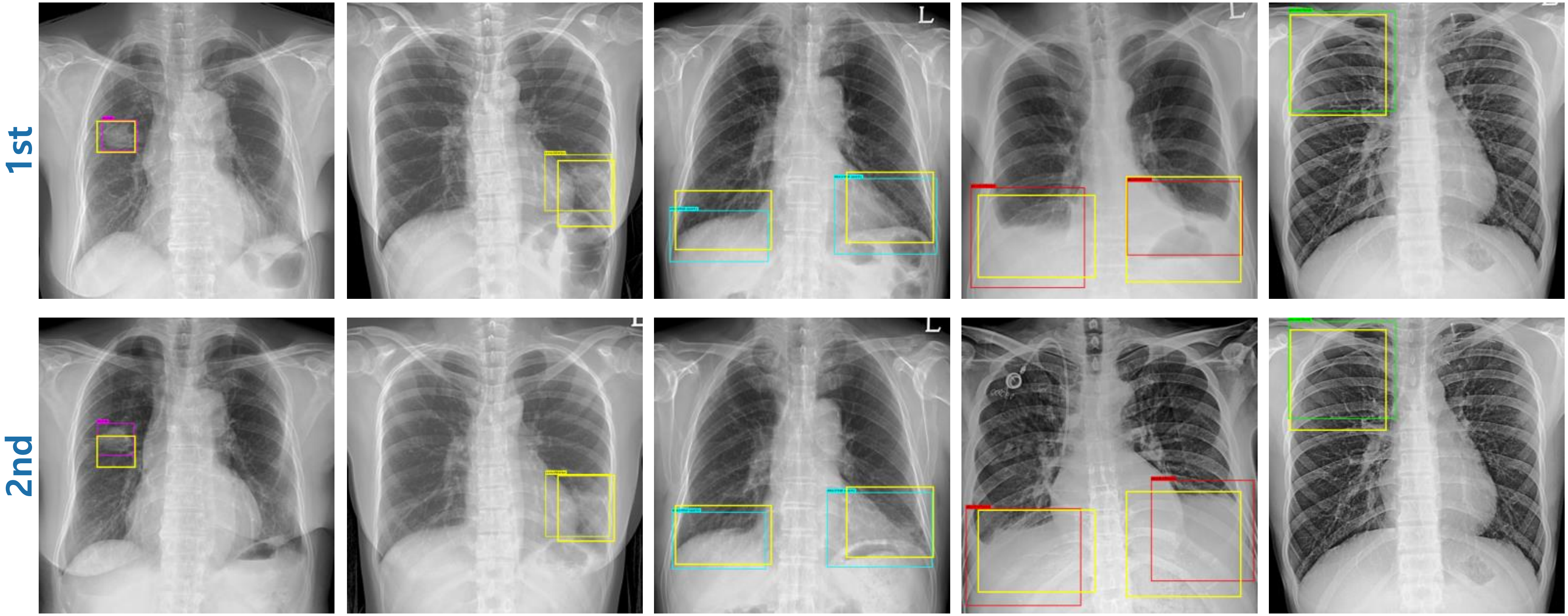

Chest PA: Reproducibility

MI2L

- Reproducibility analysis on CNN-based detection
  - Comparison of various networks

✓ YOLO v2

Nodule (N = 121)		1st P	1st N
2nd	P	94	3
2nd	N	15	9

✓ Faster RCNN

Nodule (N = 121)		1st P	1st N
2nd	P	90	8
2nd	N	11	12

✓ VUNO-net

Nodule (N = 121)		1st P	1st N
2nd	P	97	4
2nd	N	14	6

✓ Mask RCNN

Nodule (N = 121)		1st P	1st N
2nd	P	90	3
2nd	N	13	15

Chest PA: Reproducibility

- Reproducibility analysis on CNN-based detection
  - Comparison with human readers
    - ✓ Reader 1

Nodule (N = 121)		1st P	1st N
2nd	P	116	1
	N	2	2

    - ✓ Reader 2

Nodule (N = 121)		1st P	1st N
2nd	P	111	3
	N	4	3

Chest PA: Automatic delineation

- Curved line detection for cardiomegaly patients

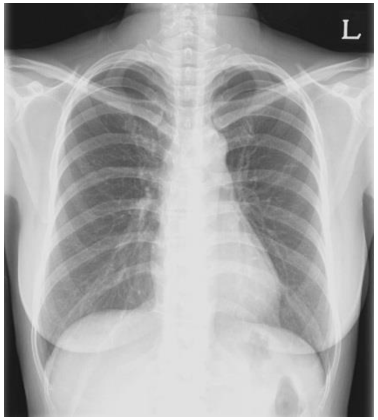

Normal

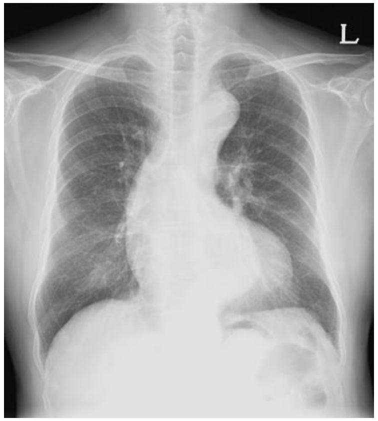

Cardiomegaly

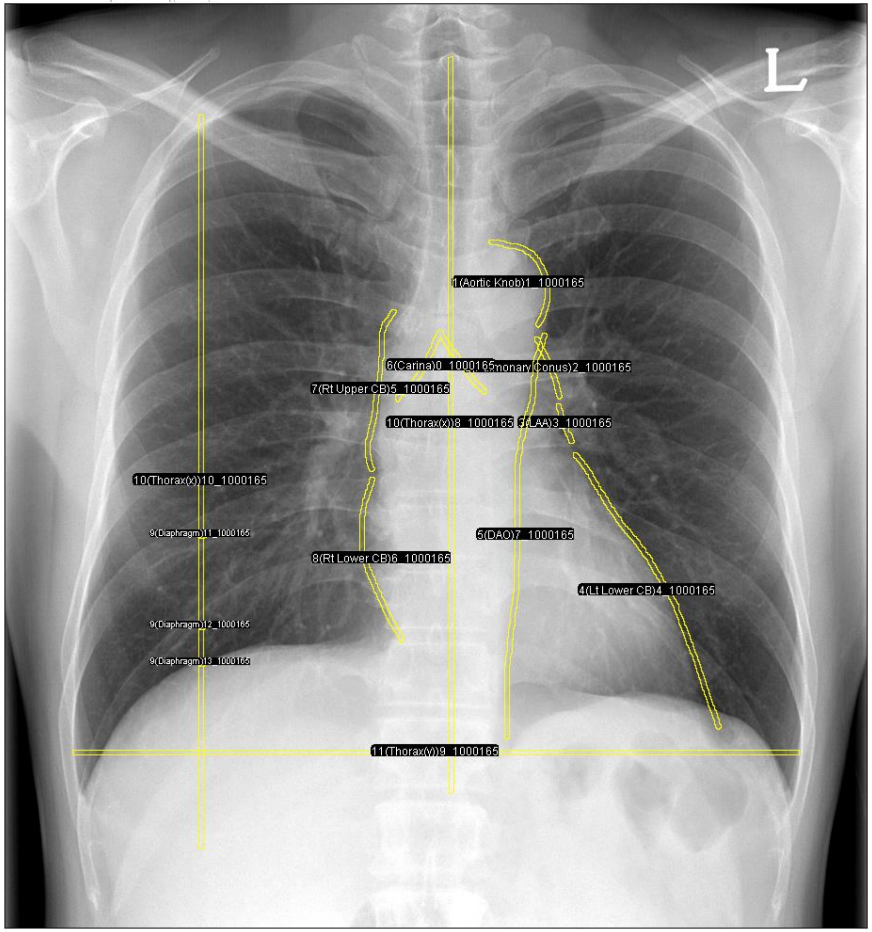

Chest PA: Automatic delineation

- Curved line detection for cardiomegaly patients
  - AMC dataset
    - ✓ Normal 1020 cases
    - ✓ cardiomegaly 1000 cases
  - 8-class curved lines
    - ✓ Aortic knob (AK)
    - ✓ Pulmonary conus (PC)
    - ✓ Left atrial appendage (LAA)
    - ✓ Descending aorta (DAO)
    - ✓ Carina (C)
    - ✓ Boundaries of left ventricle (Lt lower CB)
    - ✓ Boundaries of right atrium (Rt upper CB)
    - ✓ Boundaries of right ventricle (Rt lower CB)
    - ✓ Each line was drawn as a mask, **with 10 pixel width**

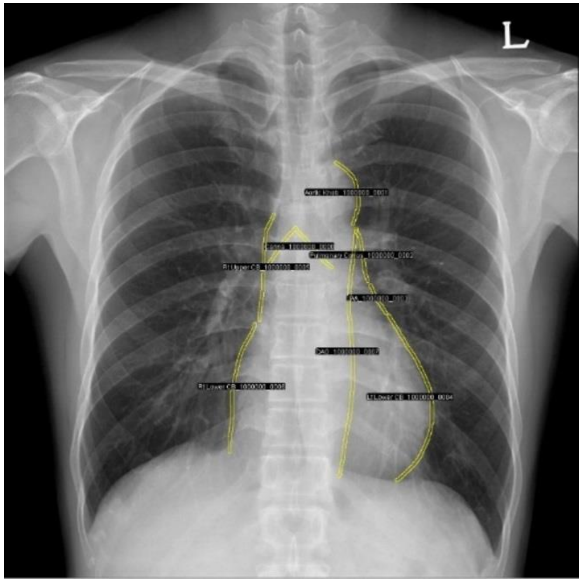

Chest PA: Automatic delineation

- Curved line detection for cardiomegaly patients
  - Network: Mask RCNN

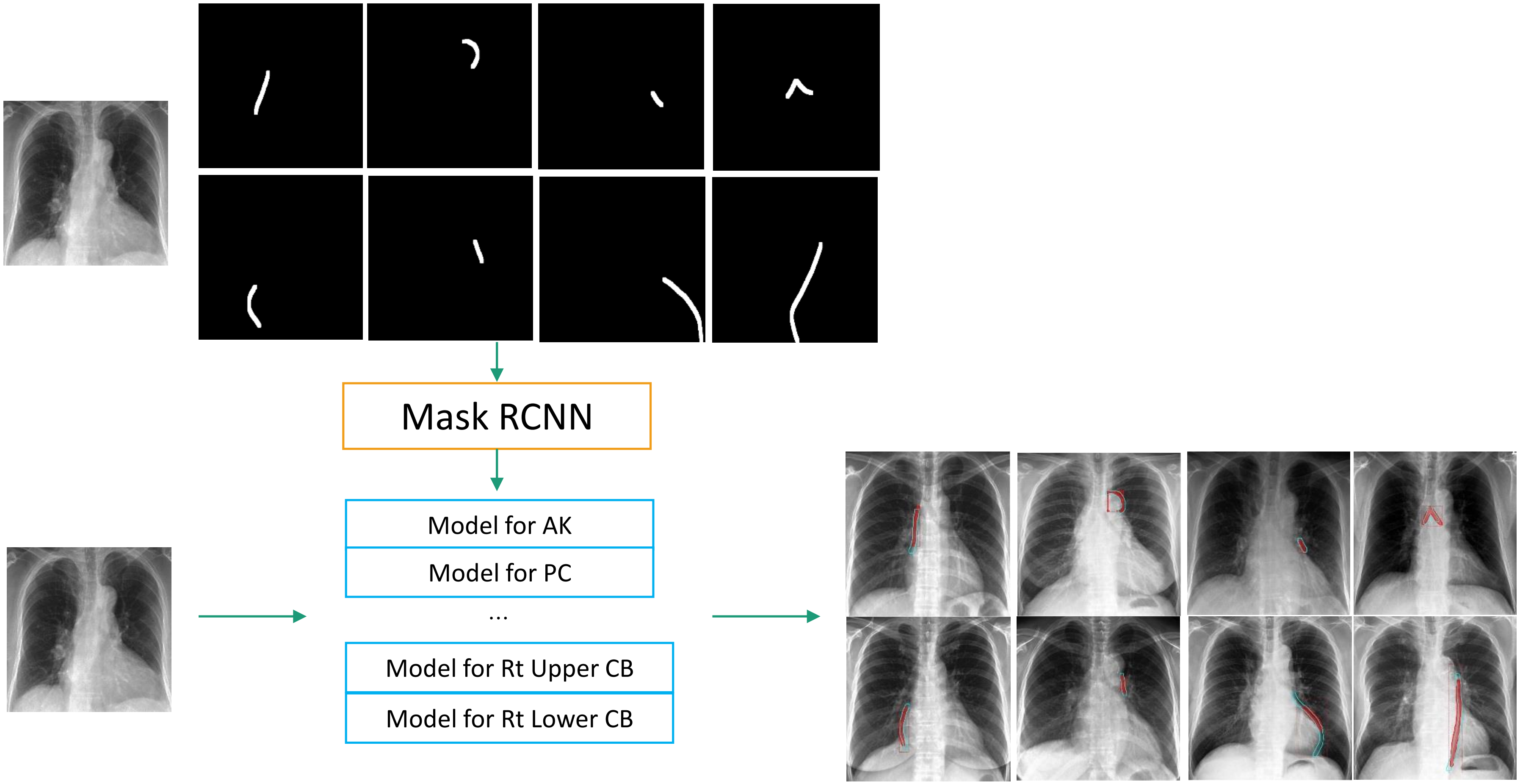

Chest PA: Automatic delineation

- Curved line detection for cardiomegaly patients
  - Results

	IOU	Detection ratio
AK	0.8029	0.9975
PC	0.5658	0.8222
LAA	0.3990	0.7171
DAO	0.6925	0.8949
Carina	0.7034	1.0000
Lt lower CB	0.7831	1.0000
Rt upper CB	0.6427	0.9927
Rt lower CB	0.6888	0.9829

Chest PA: Automatic delineation

- Curved line detection for cardiomegaly patients
  - Results

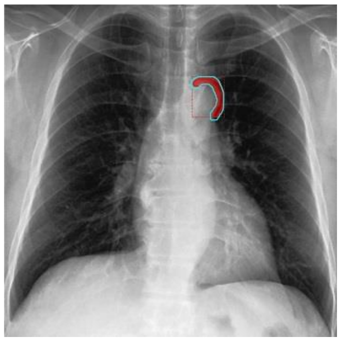

AK
0.79 ± 0.08

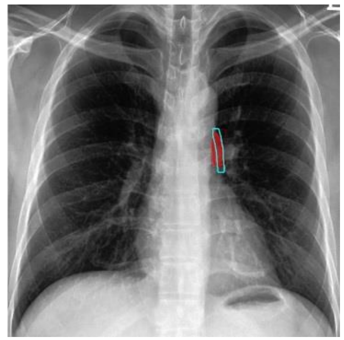

PC
0.50 ± 0.20

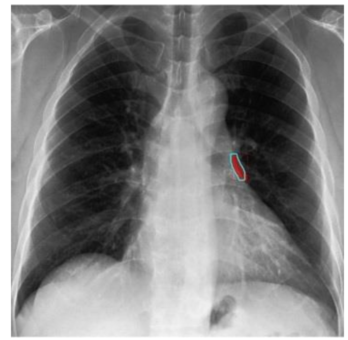

LAA
0.40 ± 0.24

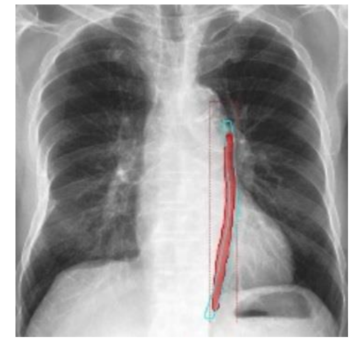

DAO
0.60 ± 0.26

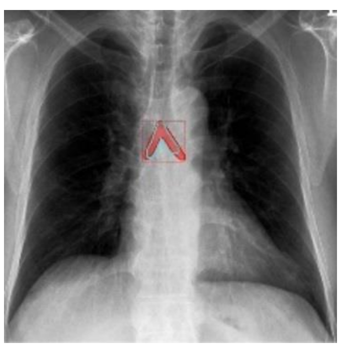

Carina
0.70 ± 0.13

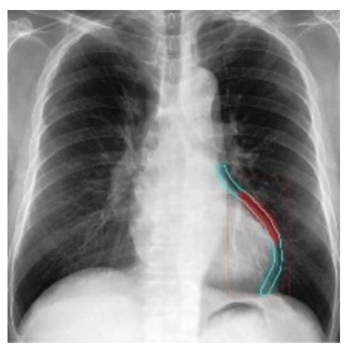

Lt lower CB
0.72 ± 0.13

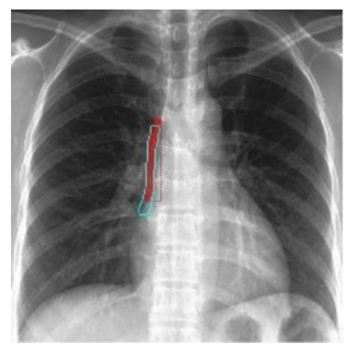

Rt upper CB
0.63 ± 0.16

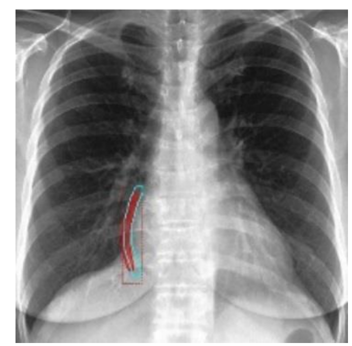

Rt lower CB
0.63 ± 0.14

Pancreas

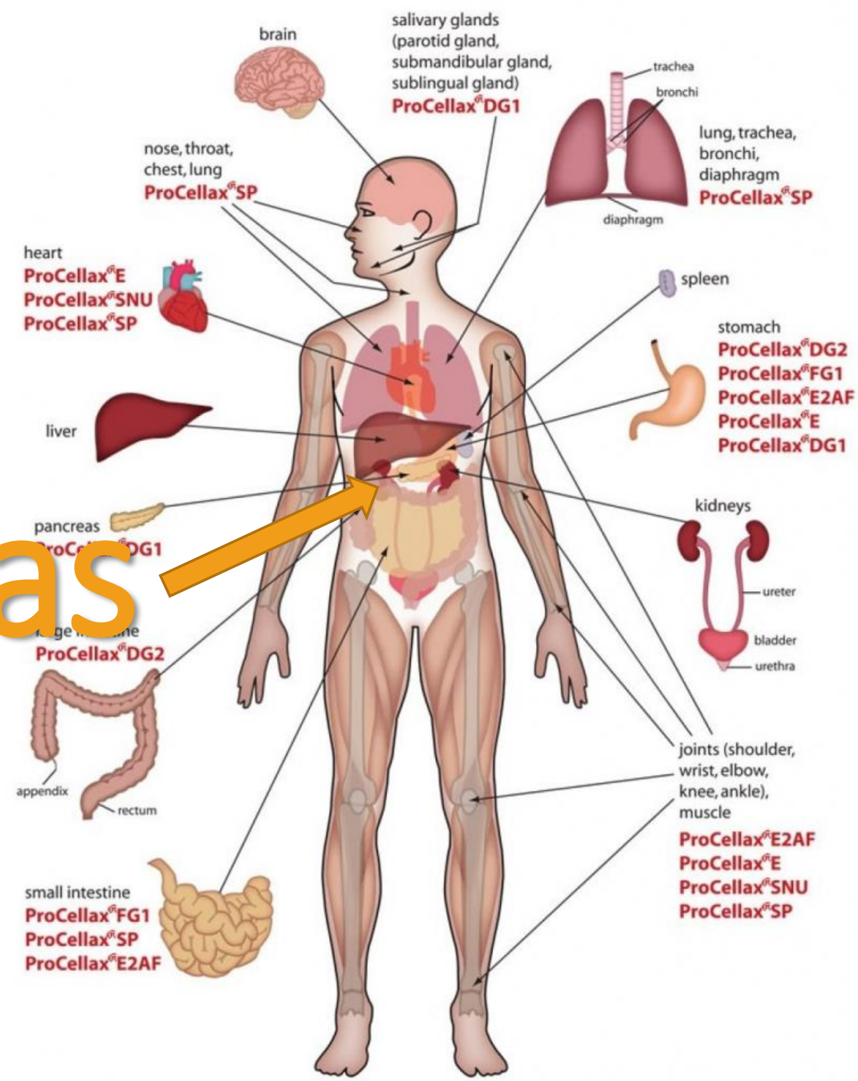
brain
salivary glands (parotid gland, submandibular gland, sublingual gland)
ProCellax®DG1
trachea
bronchi
lung, trachea, bronchi, diaphragm
ProCellax®SP
diaphragm
nose, throat, chest, lung
ProCellax®SP
heart
ProCellax®E
ProCellax®SNU
ProCellax®SP
spleen
stomach
ProCellax®DG2
ProCellax®FG1
ProCellax®E2AF
ProCellax®E
ProCellax®DG1
liver
pancreas
kidneys
ureter
bladder
urethra
ProCellax®DG2
appendix
rectum
joints (shoulder, wrist, elbow, knee, ankle), muscle
ProCellax®E2AF
ProCellax®E
ProCellax®SNU
ProCellax®SP
small intestine
ProCellax®FG1
ProCellax®SP
ProCellax®E2AF

Pancreatic Cancer

- Pancreas segmentation using domain adaptation
  - Multi-center datasets: AMC and NIH
    - ✓ AMC: 220 patients
    - ✓ NIH: 82 patients

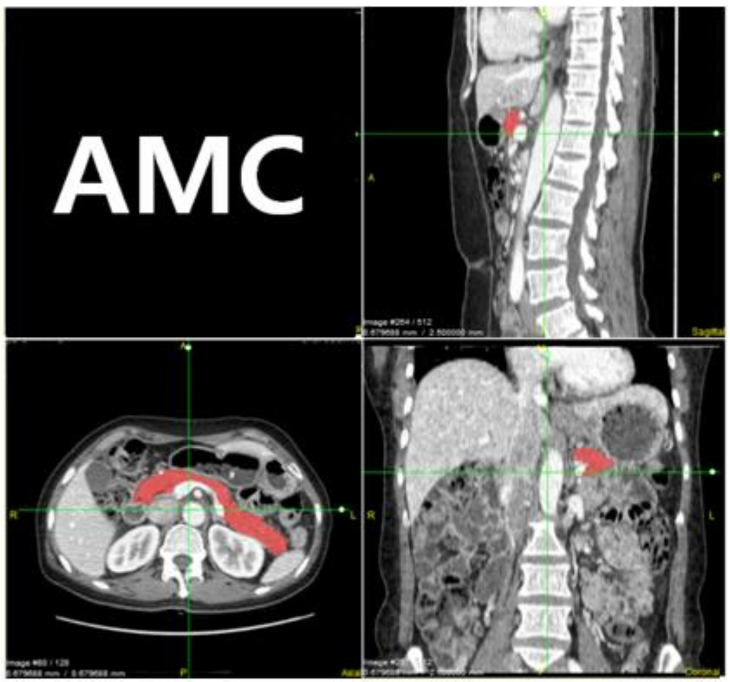

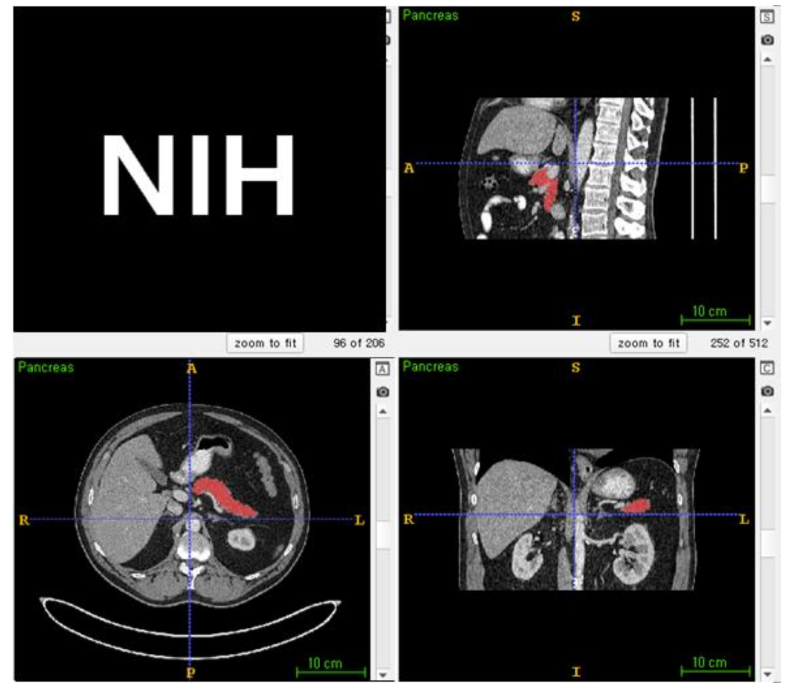

Pancreatic Cancer

- Pancreas segmentation using domain adaptation
  - Domain adaptation

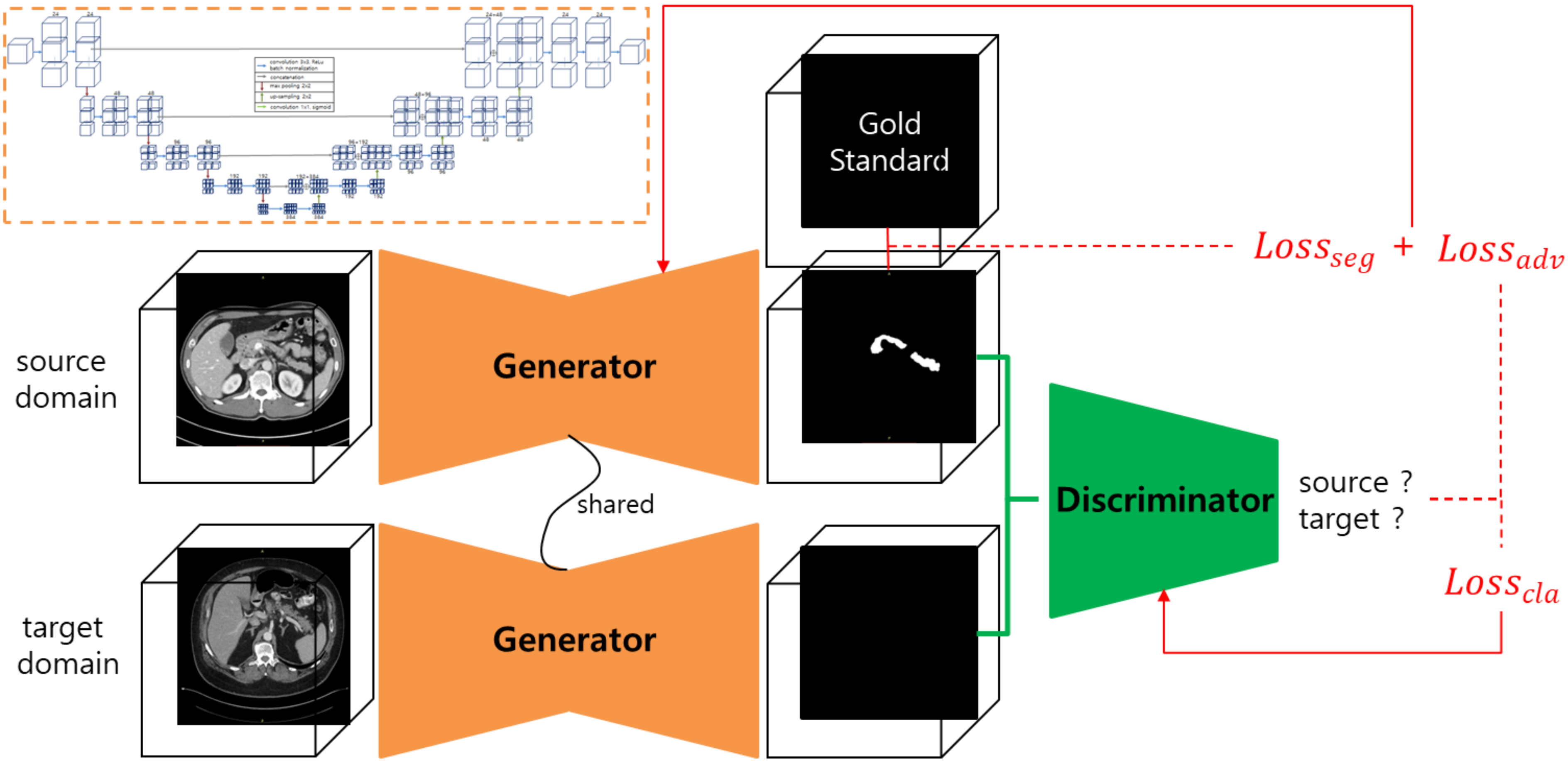

Pancreatic Cancer

- Pancreas segmentation using domain adaptation
  - Domain adaptation

Source	Target	Dice
NIH	NIH	0.7601
	AMC	0.5833
AMC (baseline)	AMC	0.8466
	NIH	0.4649
AMC (with DA)	AMC	0.8284
	NIH	0.6770

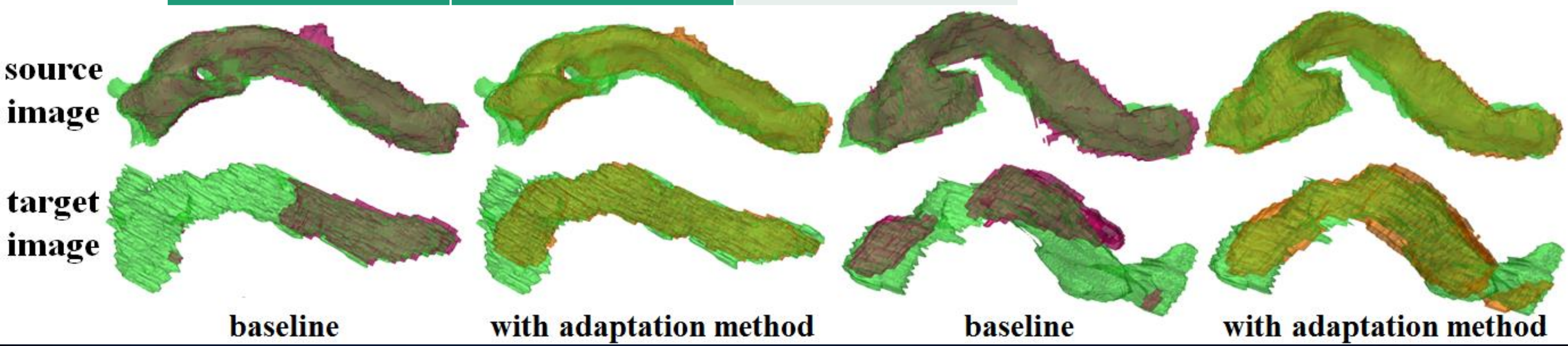

Kidney

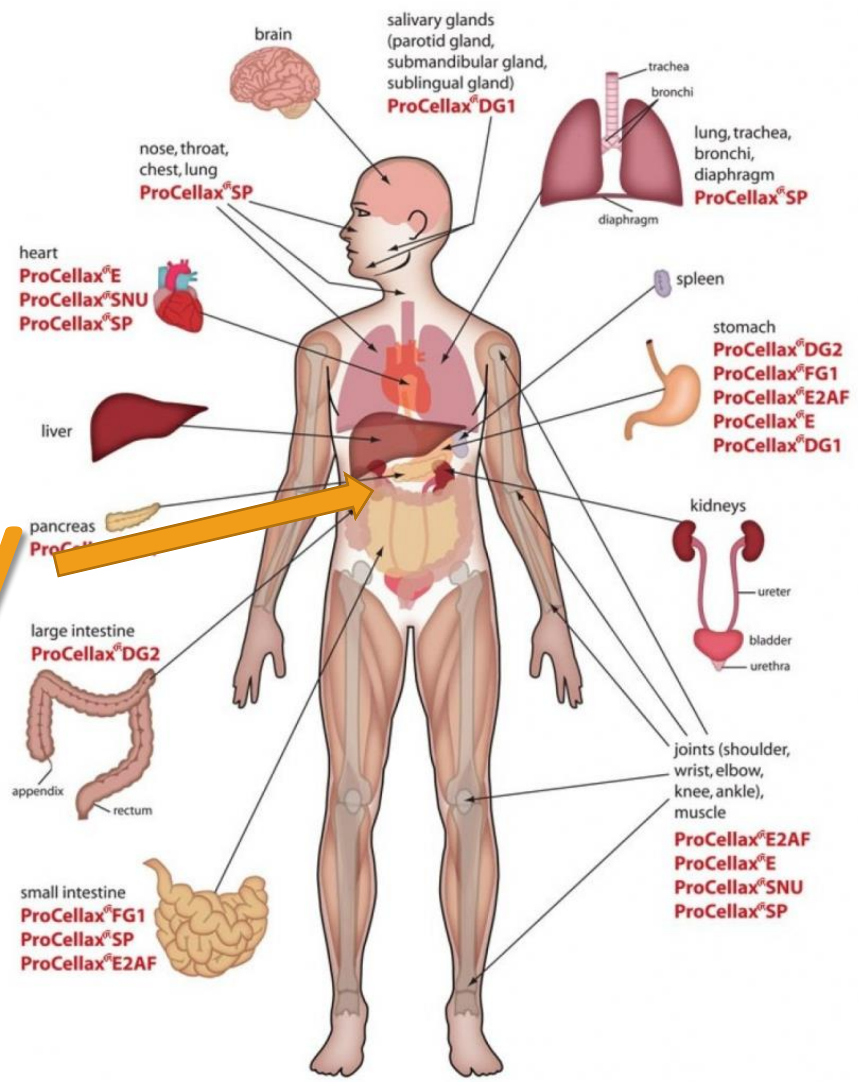

brain
salivary glands (parotid gland, submandibular gland, sublingual gland)
ProCellax®DG1
trachea
bronchi
lung, trachea, bronchi, diaphragm
ProCellax®SP
diaphragm
nose, throat, chest, lung
ProCellax®SP
heart
ProCellax®E
ProCellax®SNU
ProCellax®SP
spleen
stomach
ProCellax®DG2
ProCellax®FG1
ProCellax®E2AF
ProCellax®E
ProCellax®DG1
liver
pancreas
kidneys
ureter
bladder
urethra
large intestine
ProCellax®DG2
appendix
rectum
joints (shoulder, wrist, elbow, knee, ankle), muscle
ProCellax®E2AF
ProCellax®E
ProCellax®SNU
ProCellax®SP
small intestine
ProCellax®FG1
ProCellax®SP
ProCellax®E2AF

Kidney segmentation

- Kidney segmentation
  - Results

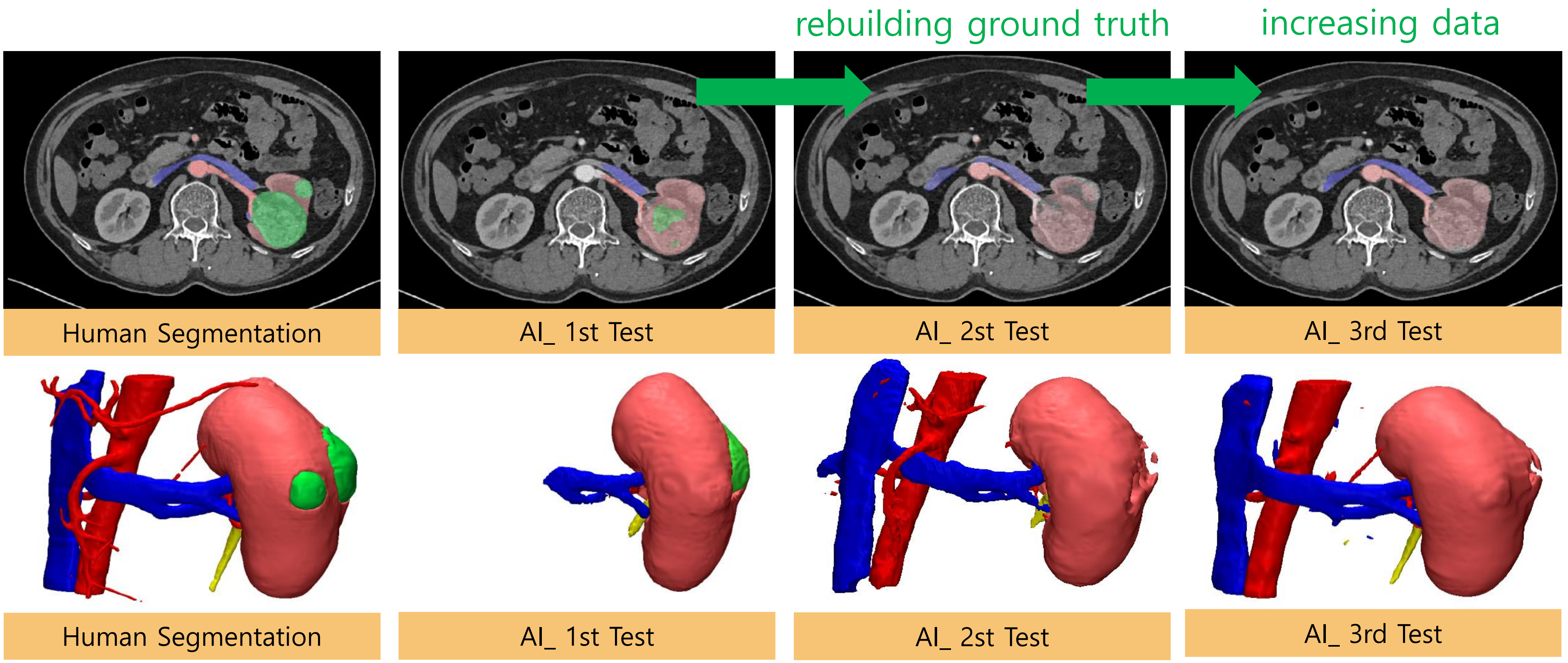

DICE	0.88	0.91	0.95

Pathology

- Survey
  - Assisting Pathologists in Detecting Cancer with Deep Learning, *Google Research Blog*, Mar. 2017

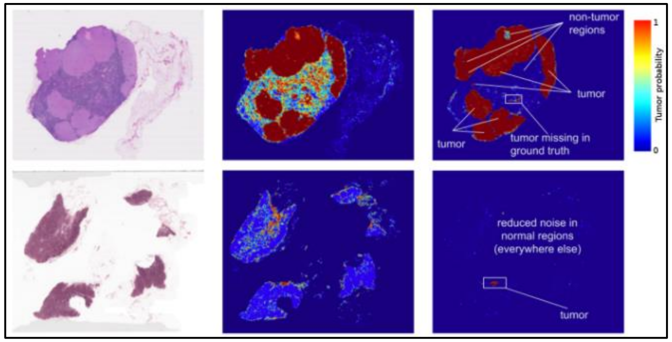

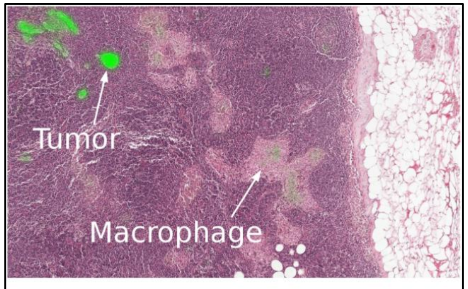

A closeup of a lymph node biopsy. The tissue contains a breast cancer metastasis as well as macrophages, which look similar to tumor but are benign normal tissue. Our algorithm successfully identifies the tumor region (bright green) and is not confused by the macrophages.

  - Diagnostic Assessment of Deep Learning Algorithms for Detection of Lymph Node Metastases in Women With Breast Cancer, *JAMA*, Dec. 2017 (from CAMELYON16)

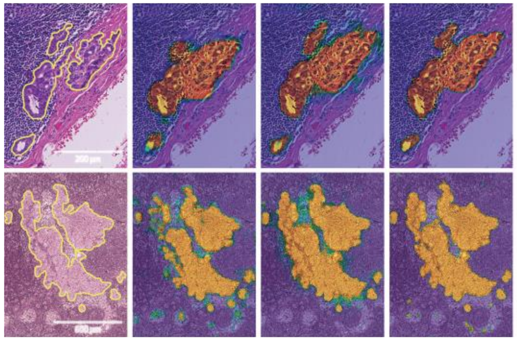

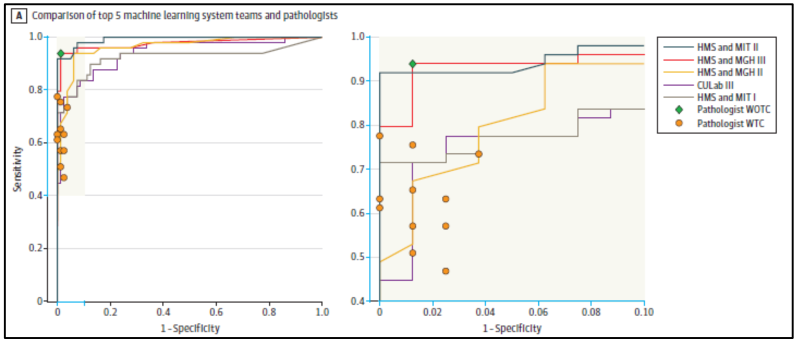

Pathology

- Peri-tubular capillary (PTC) counting

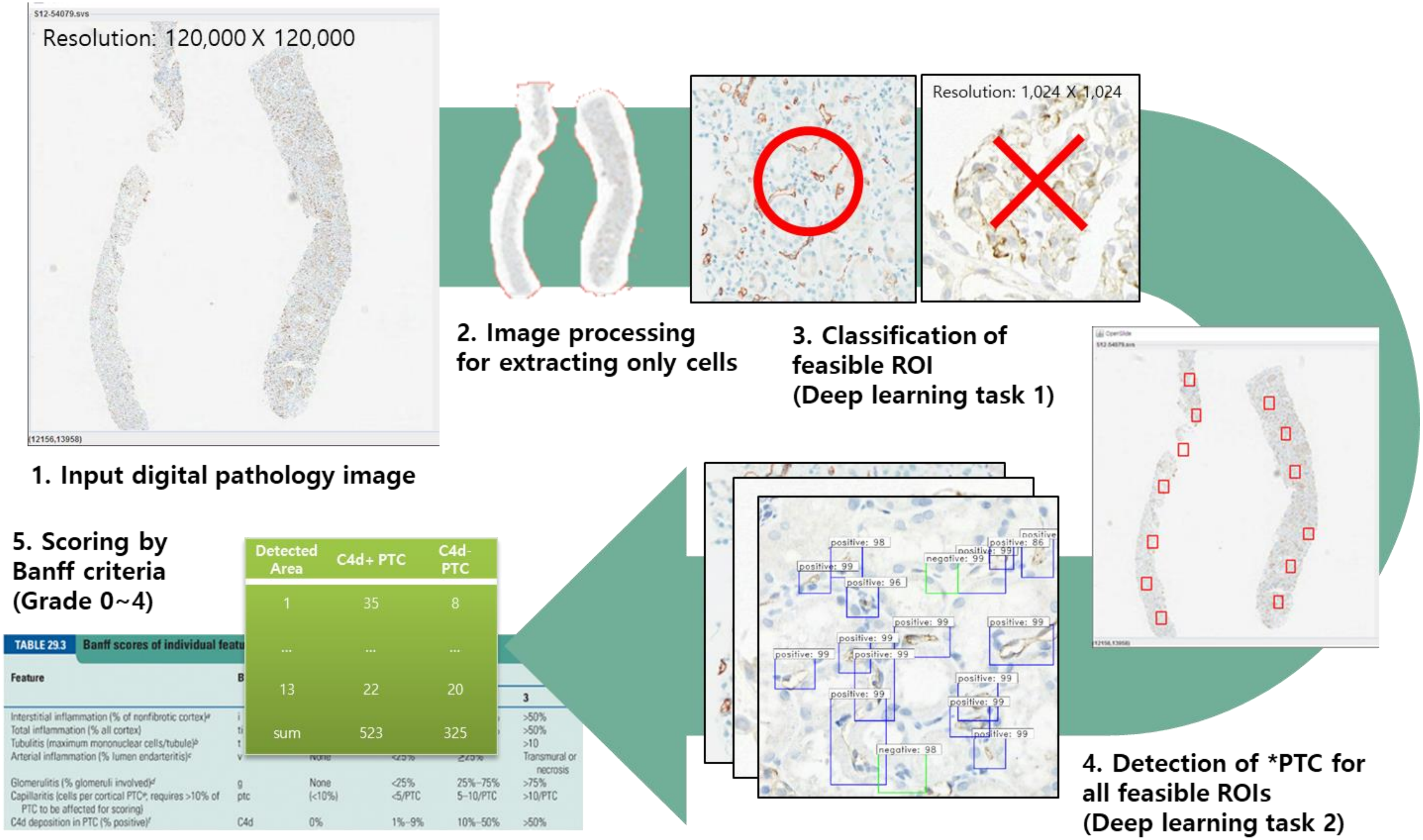

Detected Area	C4d+ PTC	C4d- PTC
1	35	8
...	...	...
13	22	20
sum	523	325

Pathology

- Peri-tubular capillary (PTC) counting
  - AMC dataset
    - ✓ Phase 1: ROI classification

Class	Training	Validation	Test
	Subset 1 (Slide 1~200)		Dataset 2 (Slide 381~480)
Feasible	1108	431	431
Non-feasible	222	100	100

    - ✓ Phase 2: PTC detection

Class	Hard labeled dataset			AI-assisted dataset		
	Training	Validation	Test	Training	Validation	Test
	Subset 1 (Slide 1~200)			Subset 2 (Slide 201~380)		
positive	423	277	202	1,503	486	496
negative	1,200	800	422	2,025	674	651

Pathology

- Peri-tubular capillary (PTC) counting
  - Phase 1: ROI classification
    - ✓ Network: Inception V3

Sensitivity	Specificity	Precision	Accuracy
0.8538	0.9550	0.9866	0.8719

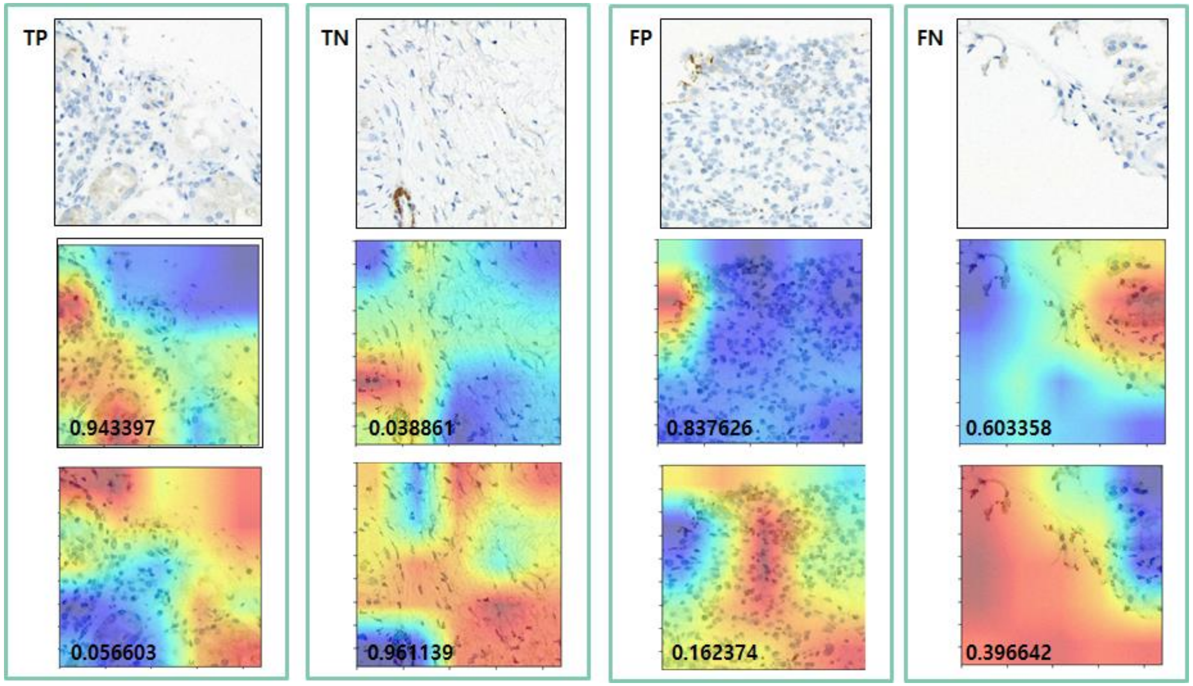

Pathology

- Peri-tubular capillary (PTC) counting
  - Phase 2: PTC detection
    - ✓ Network: Faster RCNN
    - ✓ **Margin** including various size to **include neighborhood region**

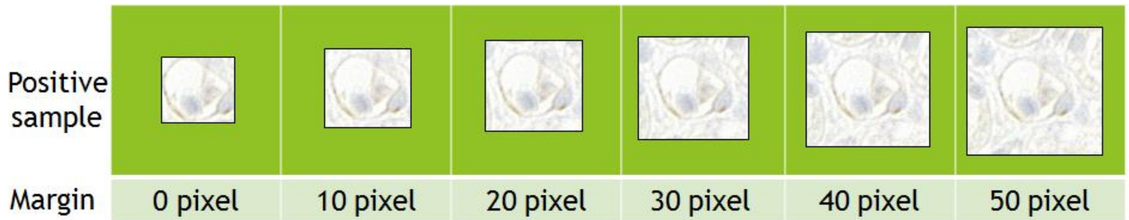

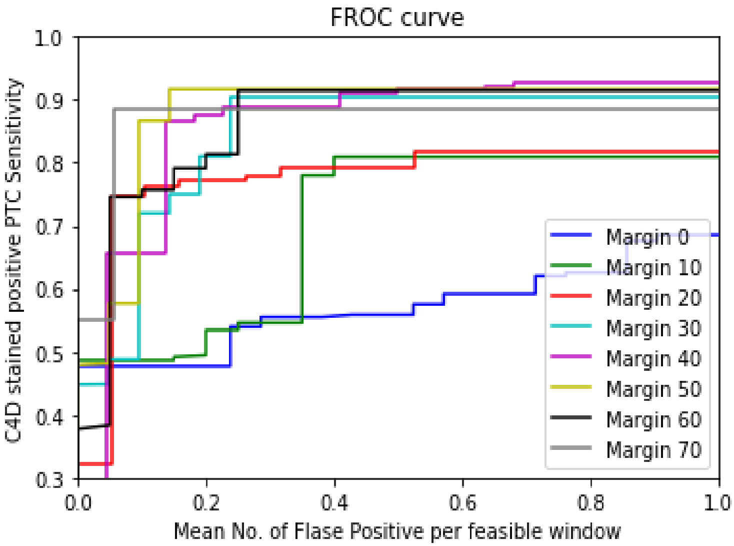

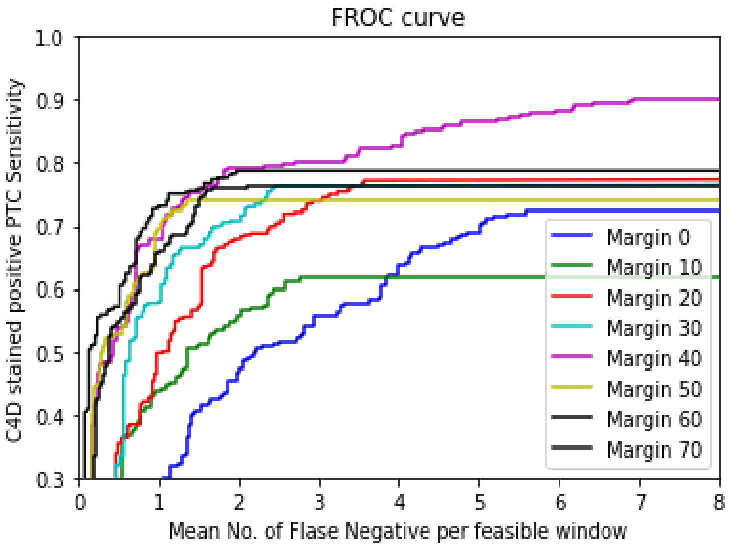

Pathology

- Peri-tubular capillary (PTC) counting
  - Feasibility of AI-assisted labeled data

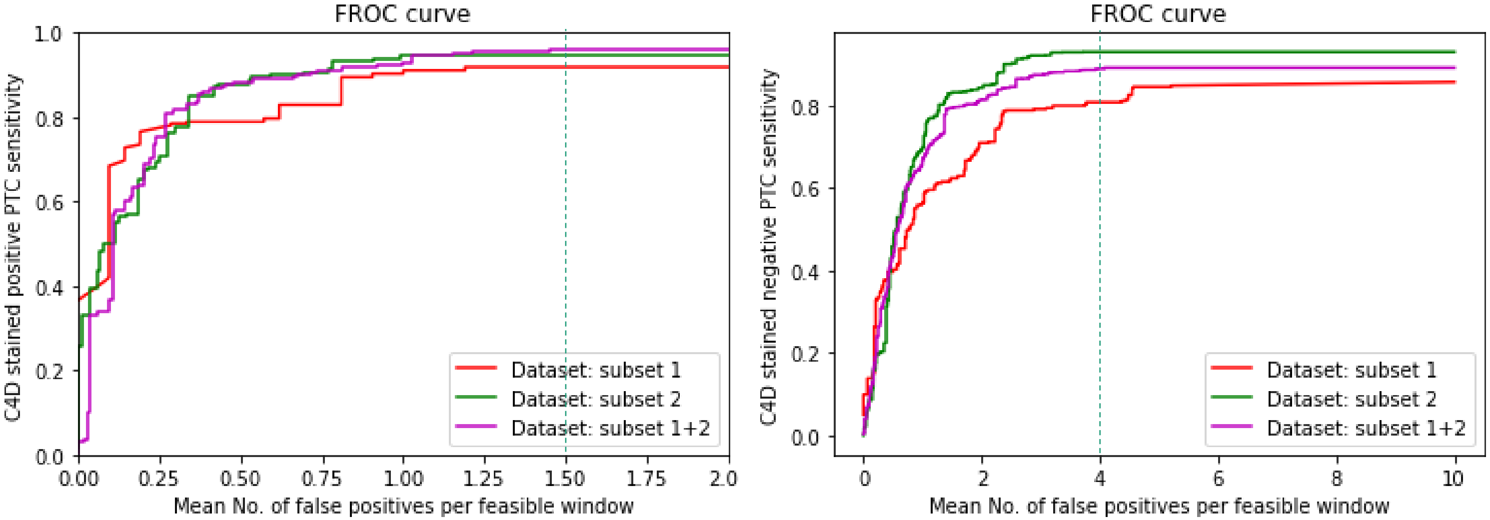

Data labeling	C4d positive	C4d negative
Hand-labeled	0.9273	0.8193
AI-assisted	0.9413	0.8864
Fusion	0.9522	0.8523

Surgical video

- Mastoidectomy
  - Scene understanding

  - Tool/structure detection

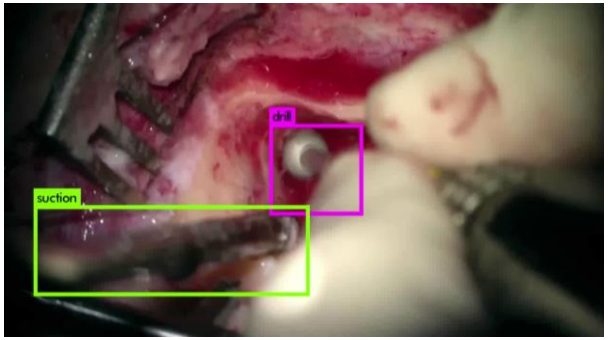

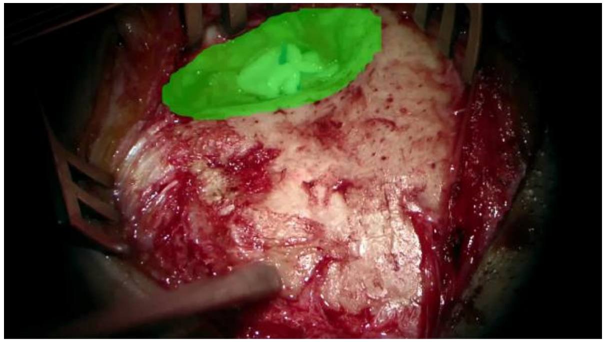

COPD deep radiomics

- Survival analysis
  - Random survival forest
  - Extraction of deep features
    - Design a CNN model for classifying 5-year survival

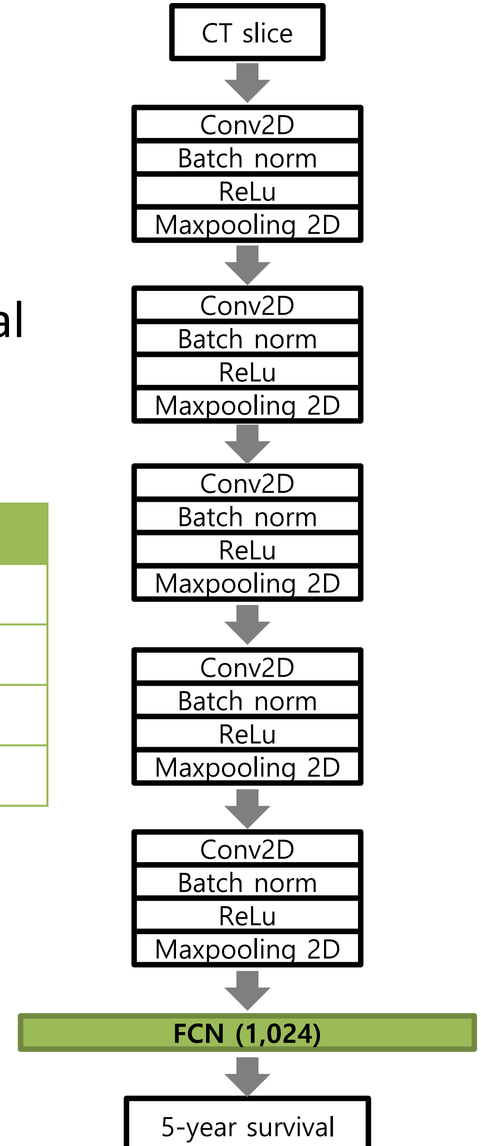

Data	C-index
Deep radiomics features (A1+A2+A3+A4+A5+A6)	**0.8412**
Demographic information	0.7688
PFT	0.7498
Handcrafted features	0.5994

AMC 영상의학과 서준범, 이상민 교수 등

CDSS on Liver Cancer

- Treatment recommender system for liver cancer
  - Patient's baseline data: 39 variables
  - 1,000 patients
  - Hierarchical decision modeling

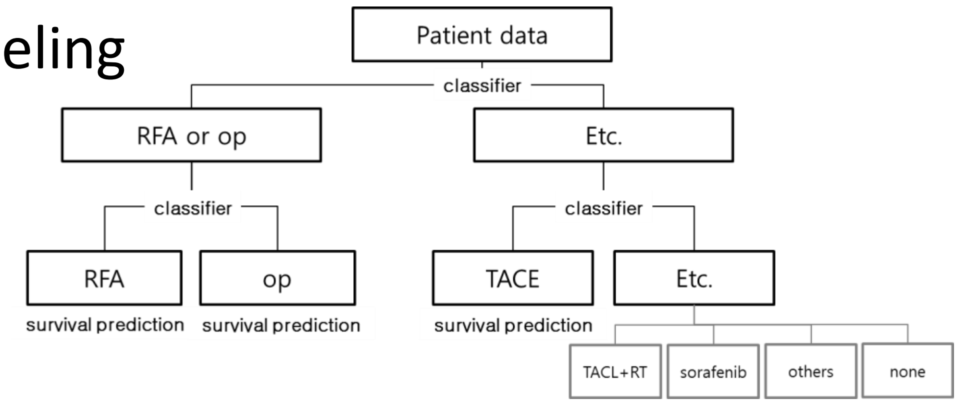

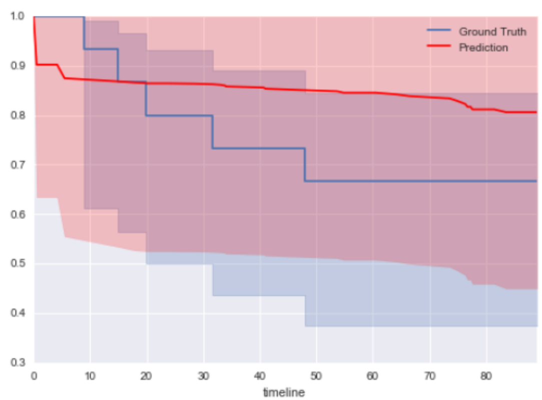

RFA

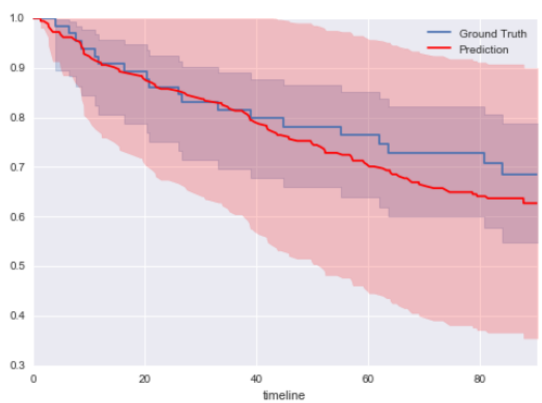

op

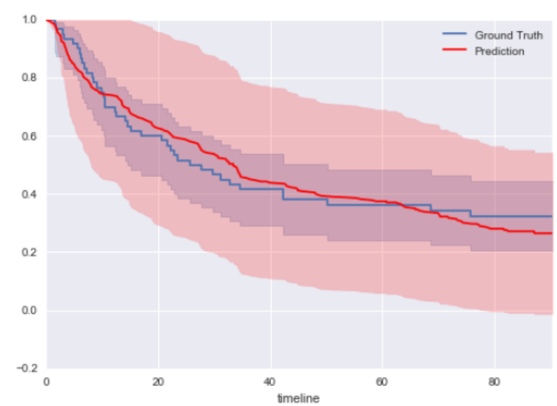

TACE

MI2RL Medical Imaging Intelligent Reality Lab

Clinical Collaborators@Asan Medical Center

Radiology: Joon Beom Seo, SangMin Lee[A,B], Dong Hyun Yang, Hyung Jin Won, Ho Sung Kim, Seung Chai Jung

Neurology: Dong-Wha Kang, Chongsik Lee, Jaehong Lee, Sangbeom Jun, Misun Kwon, Beomjun Kim

Cardiology: Jaekwan Song, Jongmin Song, Younghak Kim

Internal Medicine: Jeongsik Byeon

Pathology: Hyunjeong Go

Surgery: Bumsuk Go, JongHun Jeong, Songchuk Kim